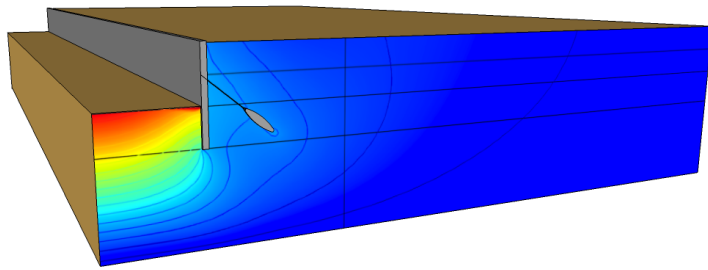




**LUND**  
UNIVERSITY



# ASSESSMENT OF FINITE ELEMENT SOFTWARES FOR GEOTECHNICAL CALCULATIONS

ALEX SPETZ

Geotechnical  
Engineering

*Master's Dissertation*



*Department of Construction Sciences*  
Geotechnical Engineering

ISRN LUTVDG/TVGT--12/5048--SE (1-100)

ISSN 0281-6679

# ASSESSMENT OF FINITE ELEMENT SOFTWARE FOR GEOTECHNICAL CALCULATIONS

Master's Dissertation by  
ALEX SPETZ

Supervisors:

Ola Dahlblom *Professor,*  
*Dept of Construction Sciences, LTH, Lund*

Per Lindh *PhD,*  
*PEAB Sverige AB*

Examiner:

Kent Persson *PhD,*  
*Dept. of Construction Sciences, LTH, Lund*

Copyright © 2011 by Geotechnical Engineering, LTH, Sweden.  
Printed by Media-Tryck LU, Lund, Sweden, May, 2012 (P).

For information, address:  
Geotechnical Engineering, LTH, Lund University, Box 118, SE-221 00 Lund, Sweden.  
Homepage: <http://www.byggvetenskaper.lth.se/geoteknik>



## Abstract

When building new constructions under ground level in cities it is important that the foundations of neighboring buildings are undisturbed. The regulations regarding soil deformations are hence very strict and conventional methods of predicting soil behavior is often too crude. Finite element calculations are therefore becoming an increasingly important tool used to predict soil behavior in and around a construction site.

When modeling soil behavior today, specialized finite element softwares for analysis of soil and rock behavior are generally used. But as the need for numerical computations within geotechnical applications increase developers of more generalized finite element softwares enter the market. It is therefore of interest to compare how a generalized finite element software handles geotechnical problems compared to a specialized geotechnical finite element software. In this study an evaluation of how a general purpose finite element software, Comsol Multiphysics, performed in geotechnical simulations compared to two finite element softwares, Plaxis 2D and Z-soil, that were developed specially for modeling of soil and geotechnical calculations.

As one important aspect to finite element calculations is the constitutive models used to capture the material behavior of the problem at hand. The two most widely used material models for simulating soil behavior are the Mohr-Coulomb criterion and the Drucker-Prager criterion, these material models have therefore been reviewed in this report. A simulation of a triaxial test has also been conducted to compare how these material models perform in the three softwares.

In the work with this report a simulation has also been carried out to compare the functionality of the three softwares for a common geotechnical application. The simulation consisted of an idealized excavation problem with a tie back retaining wall.

Modeling of a simple excavation project like the one in this report where the geometry and boundary conditions change over time is a bit more complicated and time consuming using Comsol Multiphysics compared to the two special purpose softwares. On the other hand, Comsol Multiphysics offers the user possibilities to take additional physical phenomena into account. Plaxis 2D was the software where a model could be established in the shortest time. However Plaxis 2D offers fewer options for the user than Comsol Multiphysics and Z-soil. Using Z-soil the user is given more complex alternatives to model constructions than in Plaxis 2D,

but the software is on the other hand somewhat more difficult to learn. It also takes longer time to establish a model in Z-soil than in Plaxis 2D.

From the calculations no major differences in soil deformation or forces in the ground anchoring could be identified from the three softwares, although some variations were observed.

# Preface

This master dissertation was carried out at the Department of Construction Science at LTH, Lund University, from June 2011 to May 2012.

First I would like to thank my supervisors professor Ola Dalhblom, at the Department of Construction Science and Per Lindh, Peab AB, for their support, patience and encouragement. I would also like to thank the staff of the Department of Construction Science, the Max-Lab staff and the fellow students I sheared office with for brightening up the days with interesting discussions.

I would also like to express my gratitude and love to my parents, Charlie and Solveig, for their endless support during my entire education.

Alex Spetz  
Lund, May 2012



---

# Contents

<b>1 Introduction</b>	<b>1</b>
1.1 Background . . . . .	1
1.2 Objective and Method . . . . .	1
1.3 Disposition . . . . .	2
<b>2 Strain</b>	<b>5</b>
2.1 Strain tensor . . . . .	5
2.2 Strain invariants . . . . .	10
<b>3 Stress</b>	<b>13</b>
3.1 Stress tensor . . . . .	13
3.2 Stress invariants . . . . .	15
3.3 Various states of stress . . . . .	19
<b>4 Constitutive relation</b>	<b>21</b>
4.1 Linear elasticity . . . . .	21
4.2 Plasticity theory . . . . .	22
<b>5 Soil behavior</b>	<b>37</b>
5.1 Soil strength . . . . .	37
5.2 Mohr-Coloumb . . . . .	41
5.3 Drucker-Prager . . . . .	44
5.4 Elliptic cap . . . . .	47
<b>6 Software introduction</b>	<b>49</b>
6.1 Introduction of Plaxis 2D . . . . .	49
6.2 Introduction of Z-Soil . . . . .	50
6.3 Introduction of COMSOL Multiphysics . . . . .	50
6.4 Sign convention . . . . .	50
6.5 Soil material models . . . . .	51

6.6	Simulation of Triaxial test . . . . .	56
<b>7</b>	<b>Excavation with a tie back retaining wall</b>	<b>63</b>
7.1	Material Parameters . . . . .	64
7.2	Finite element model . . . . .	65
7.3	Plaxis . . . . .	68
7.4	Z-soil . . . . .	72
7.5	Comsol Multiphysics . . . . .	78
7.6	Results . . . . .	82
7.7	Discussion . . . . .	90
<b>8</b>	<b>Conclusions and suggestions for further work</b>	<b>93</b>
<b>9</b>	<b>Bibliography</b>	<b>97</b>

# 1 Introduction

## 1.1 Background

All constructions, whether if it is roads, bridges, canals, dams, or buildings have one thing in common, they are built on, in, or with soil or rock. Hence the behavior of these materials has great influence on the success of any construction (Mitchell and Soga; 2005). Moreover, it is becoming increasingly important to be able to predict the behavior of earth-materials when new constructions are being built in the proximity of existing constructions. It is therefore imperative to have good understanding on how soils and rocks behave when subjected to new loading situations.

One growing tool to help predicting the behavior of soils and rocks are finite element calculations. Today there are a number of developers of different finite element softwares on the market and specialized programs for analysis of soil and rock behavior exists. As the need for numerical computations within geotechnical applications increase developers of more generalized finite element softwares enters the market. It is therefore of interest to compare how a generalized software handles geotechnical problems compared to a specialized geotechnical software.

## 1.2 Objective and Method

The main objective of this Master's dissertation is to evaluate how a generalized finite element software, Comsol Multiphysics, compares to two specialized finite element softwares, namely Plaxis 2D and Z-soil, in geotechnical calculations.

As one important aspect to finite element calculations is the material models used

to simulate the material behavior of the problem at hand. Therefore, two of the most common material models used to simulate soil behavior, namely the Mohr-Coulomb criterion and the Drucker-Prager criterion will be reviewed. As soil in contrast to most other construction materials is allowed to enter into the plastic region during deformation, the material models used to model soil behavior use the theory of plasticity and hence this report starts off by an extensive review of the theory of plasticity.

To compare the functionality of the three softwares a simulation of an idealized geotechnical problem will be performed. The problem consists of an excavation performed in steps, with a retaining wall that is anchored into the soil with a pre-stressed steel bar.

## 1.3 Disposition

This report can be divided into two sections, starting with Chapters 2–5 containing a theoretical review of the theory of plasticity and soil properties. The second part of the report, Chapters 6–8, contains the evaluation of the finite element softwares.

Looking at the structure of the report it is divided into the following chapters:

Chapter 2 introduces the strain expression and the strain invariants used in soil mechanics and the theory of plasticity.

Chapter 3 introduces the stress expression and the stress invariants used in soil mechanics and the theory of plasticity.

Chapter 4 contains a review of the theory of plasticity.

Chapter 5 describes some soil properties and material models used to simulate soil behavior.

Chapter 6 introduces the three finite element softwares compared in this report. The chapter ends with a simulation of a triaxial test, to evaluate possible differences in the Mohr-Coulomb and Drucker-Prager criterions.

Chapter 7 contains the simulation procedure and results gained from the idealized excavation problem.

Chapter 8 will point out some of the pros and cons that have been experienced using each of the three softwares for geotechnical calculations. The chapter ends with a suggestion for further work.

Chapter 9 contains the bibliography.



## 2 Strain

To evaluate the differences between the finite element softwares dealt with in this report, it is essential to have knowledge of how the softwares handle various material models. To discuss the pros and cons of the differences between the material models later on, this and the following chapters will handle the basics of constitutive modeling. This will be done by explaining the stress and strain expressions after which a general linear constitutive model will be discussed. Geotechnical material though, are generally not showing a linear behavior, it is therefore necessary to discuss non-linear material relations as well.

### 2.1 Strain tensor

In mechanics the deformations of a continuous body is commonly described by the strain quantity, which describes a deformation in terms of relative displacement of a material point, i.e. a particle, in a body. Consider a point, A, in an undeformed body that can be described with coordinates  $(x, y, z)$ , or as done in this report with index notation  $(x_1, x_2, x_3)$ , if the body is deformed the point, A, will be moved to A\* and described by the coordinates  $(x_1^*, x_2^*, x_3^*)$ , where

$$x_i^* = x_i + u_i \tag{2.1}$$

$u_1, u_2$  and  $u_3$  describing the displacements in the  $x_1, x_2$  and  $x_3$  directions over time respectively, i.e.  $x_1^* = x_1 + u_1(x_1, t)$ . The displacements are often written in vector form as

$$\mathbf{u} = \begin{bmatrix} u_1 \\ u_2 \\ u_3 \end{bmatrix}$$

or written with index notation

$$u_i = u_i(x_i, t)$$

Consider an adjacent point, B, in the body as shown in Figure 2.1. Let the point be described with coordinates  $(x_i + dx_i)$ , where  $dx_i$  denotes the distance between point A and B prior to deformation. Point B will in conformity with point A be moved to B\* after a deformation of the body. The displacements of point B\* will then be given by  $du_i$ , written out as

$$\begin{aligned} du_1 &= \frac{\partial u_1}{\partial x_1} dx_1 + \frac{\partial u_1}{\partial x_2} dx_2 + \frac{\partial u_1}{\partial x_3} dx_3 \\ du_2 &= \frac{\partial u_2}{\partial x_1} dx_1 + \frac{\partial u_2}{\partial x_2} dx_2 + \frac{\partial u_2}{\partial x_3} dx_3 \\ du_3 &= \frac{\partial u_3}{\partial x_1} dx_1 + \frac{\partial u_3}{\partial x_2} dx_2 + \frac{\partial u_3}{\partial x_3} dx_3 \end{aligned} \quad (2.2)$$

written in the more compact index form as,

$$du_i = u_{i,j} dx_j$$

where  $u_{i,j}$  is called the *displacement gradient*, defined as

$$u_{i,j} = \frac{\partial u_i}{\partial x_j} \quad (2.3)$$

The distance from point A to B prior to deformation, is as mentioned given by  $dx_i = (dx_1, dx_2, dx_3)$ , se Figure 2.1. In the following the length of the vector from A to B will be denoted  $|\overrightarrow{AB}|$ .

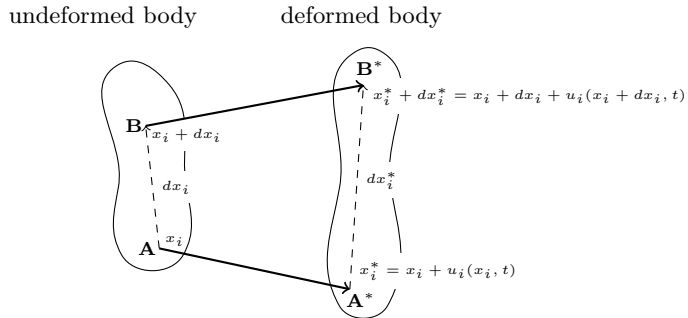


Figure 2.1: Illustration of displacements of neighboring material points.

As illustrated in Figure 2.1 the vector  $dx_i$  changes to  $dx_i^*$  due to deformation and can with the help of (2.1) be written as

$$dx_i^* = dx_i + du_i = (\delta_{ij} + u_{i,j})dx_j \quad (2.4)$$

Using the same notation as in the undeformed state, the length of the vector from  $A^*$  to  $B^*$  is denoted  $|\overrightarrow{A^*B^*}|$ , it will then become clear that

$$|\overrightarrow{A^*B^*}|^2 = (\delta_{kj} + u_{k,j})(\delta_{ki} + u_{k,i})dx_jdx_i \quad (2.5)$$

Using that  $|\overrightarrow{AB}|^2 = dx_jdx_j$  and that  $dx_jdx_j = dx_idx_j\delta_{ij}$  together with (2.5) the difference between  $|\overrightarrow{A^*B^*}|^2$  and  $|\overrightarrow{AB}|^2$  can be written as

$$|\overrightarrow{A^*B^*}|^2 - |\overrightarrow{AB}|^2 = (u_{i,j} + u_{j,i} + u_{k,i}u_{k,j})dx_jdx_i \quad (2.6)$$

This equation may be rewritten with the *Green strain tensor*, denoted  $E_{ij}$ , as

$$|\overrightarrow{A^*B^*}|^2 - |\overrightarrow{AB}|^2 = 2dx_iE_{ij}dx_j \quad (2.7)$$

where

$$E_{ij} = \frac{1}{2}(u_{i,j} + u_{j,i} + u_{k,i}u_{k,j}) \quad (2.8)$$

The Green strain tensor is a second-order tensor and symmetric and it was first introduced by Green in 1841. However, in this report a simplification will be done regarding the displacement gradient. From here and on only the *small displacement gradient* will be considered, consequently the quadratic term of (2.8) can be ignored. This simplification can be expressed by the *small strain tensor*

$$\varepsilon_{ij} = \frac{1}{2}(u_{i,j} + u_{j,i}) \quad (2.9)$$

Which is also a second-order tensor, i.e. is symmetric  $\varepsilon_{ij} = \varepsilon_{ji}$ . It is the strain that will be used in the following.

### 2.1.1 Normal strains

Using the small strain tensor the diagonal terms called the *normal strains* will now be investigated further, starting by establishing that (2.7) can be written

as

$$\frac{|\overrightarrow{A^*B^*}|^2 - |\overrightarrow{AB}|^2}{|\overrightarrow{AB}|^2} = 2 \frac{dx_i}{|\overrightarrow{AB}|} \varepsilon_{ij} \frac{dx_j}{|\overrightarrow{AB}|} \quad (2.10)$$

If the deformation illustrated in Figure 2.1 is considered, where the length of  $dx_i$  is given from  $|\overrightarrow{AB}|$ , a unit vector in the direction of  $dx_i$  can be formed as

$$n_i = \frac{dx_i}{|\overrightarrow{AB}|} \quad (2.11)$$

It then follows that (2.10) can be rewritten as

$$\frac{|\overrightarrow{A^*B^*}|^2 - |\overrightarrow{AB}|^2}{2|\overrightarrow{AB}|^2} = n_i \varepsilon_{ij} n_j \quad (2.12)$$

Since all displacement gradients are assumed to be small, the length  $|\overrightarrow{A^*B^*}|$  will be close to  $|\overrightarrow{AB}|$  which implies that (2.12) can be approximated

$$\frac{(|\overrightarrow{A^*B^*}| + |\overrightarrow{AB}|)(|\overrightarrow{A^*B^*}| - |\overrightarrow{AB}|)}{2|\overrightarrow{AB}|^2} \approx \frac{2|\overrightarrow{AB}|(|\overrightarrow{A^*B^*}| - |\overrightarrow{AB}|)}{2|\overrightarrow{AB}|^2}$$

With the help of this approximation the *relative elongation* of the vector  $|\overrightarrow{AB}|$  will be determined by

$$\varepsilon = \frac{|\overrightarrow{A^*B^*}| - |\overrightarrow{AB}|}{|\overrightarrow{AB}|} \quad (2.13)$$

Combining (2.12) and (2.13) the definition of the normal strains is obtained as

$$\varepsilon = n_i \varepsilon_{ij} n_j$$

Inserting  $n_i = (1, 0, 0)$  it becomes clear that the  $\varepsilon_{11}$  term will be obtained, and in the corresponding manner  $\varepsilon_{22}$  and  $\varepsilon_{33}$  is obtained when  $n_i = (0, 1, 0)$  or  $n_i = (0, 0, 1)$  (Ottosen and Ristinmaa; 2005)

$$\begin{aligned}\varepsilon_{11} &= \frac{1}{2} \left( \frac{\partial u_1}{\partial x_1} + \frac{\partial u_1}{\partial x_1} \right) \\ \varepsilon_{22} &= \frac{1}{2} \left( \frac{\partial u_2}{\partial x_2} + \frac{\partial u_2}{\partial x_2} \right) \\ \varepsilon_{33} &= \frac{1}{2} \left( \frac{\partial u_3}{\partial x_3} + \frac{\partial u_3}{\partial x_3} \right)\end{aligned}\tag{2.14}$$

### 2.1.2 Shear strains

The off-diagonal parts of the strain tensor can be described by studying the change in angle between neighboring material points due to deformation. If the material points given by A, B and C in Figure 2.2 are considered and letting  $A^*$ ,  $B^*$  and  $C^*$  describe the points after deformation, it can then be seen that as the deformation occurs the angle between the lines AB and AC in Figure 2.2 will change due to deformation.

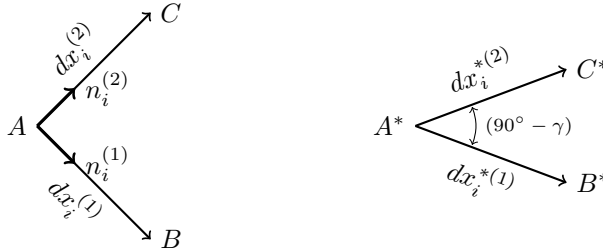


Figure 2.2: Illustration of how the orthogonal angle changes due to deformation.

From Figure 2.2 it is evident that an expression for the angle  $90^\circ - \gamma$  can be formed as

$$\cos(90^\circ - \gamma) = \frac{dx_i^{*(1)} \cdot dx_i^{*(2)}}{|A^*B^*| |A^*C^*|}\tag{2.15}$$

Where  $|A^*B^*|$  and  $|A^*C^*|$  denote the length of the vectors  $dx_i^{*(1)}$  and  $dx_i^{*(2)}$  respectively. Inserting the expression for  $dx_i^*$  from (2.4) into (2.15) the angle  $\gamma$

will be given from

$$\sin \gamma = (\delta_{jk} + u_{k,j} + u_{j,k} + u_{i,j}u_{i,k}) \frac{dx_j^{(1)}}{|\overrightarrow{A^*B^*}|} \frac{dx_k^{(2)}}{|\overrightarrow{A^*C^*}|} \quad (2.16)$$

As only small strains are assumed the quadratic term of (2.16) can be ignored, furthermore an approximation that  $|\overrightarrow{A^*B^*}| \approx |\overrightarrow{AB}|$  and  $|\overrightarrow{A^*C^*}| \approx |\overrightarrow{AC}|$  may be done. It follows that unit vectors,  $m_i$  and  $n_i$ , can be formed in conformity with (2.11), inserting the unit vectors  $m_i$  and  $n_i$  into (2.16) it reduces to

$$\sin \gamma = 2m_i \varepsilon_{ij} n_j$$

The small strain approximation also gives that  $\sin \gamma \approx \gamma$  which leads to the final expression for the off-diagonal parts of the strain tensor

$$\gamma = 2m_i \varepsilon_{ij} n_j \quad (2.17)$$

or written in a different manner as,

$$\gamma_{nm} = 2\varepsilon_{nm}$$

The decrease of the angle from the configuration state is thus described by the off-diagonal parts of the strain tensor. This can be showed by looking at an example where  $m_i = (1, 0, 0)$  and  $n_j = (0, 1, 0)$  giving that  $\gamma = 2\varepsilon_{12}$ . Using different directions for  $m$  and  $n$  one can evaluate  $2\varepsilon_{13}$  and  $2\varepsilon_{23}$  in a similar manner. These terms of the strain tensor that describe the shear of the material, i.e. the material distortion are hence called *shear strains*, (Ottosen and Ristinmaa; 2005).

With both the diagonal and off-diagonal terms of the strain tensor described it can be written in its full form as

$$\varepsilon_{ij} = \begin{bmatrix} \varepsilon_{11} & \varepsilon_{12} & \varepsilon_{13} \\ \varepsilon_{21} & \varepsilon_{22} & \varepsilon_{23} \\ \varepsilon_{31} & \varepsilon_{32} & \varepsilon_{33} \end{bmatrix} \quad (2.18)$$

## 2.2 Strain invariants

When discussing constitutive relations and yield criteria it is often advantageous to use invariants to describe the relations, that is quantities that take the same

values independent of the coordinate system. In this part the strain tensor invariants will be discussed. In this report though, the strain invariants will not be derived and the reader is referred to other literature on the topic for further studies.

### 2.2.1 Principal strains

The *Principal strains*  $(\varepsilon_1, \varepsilon_2, \varepsilon_3)$  represents the maximum elongation of an element and can be determined using the definition for the relative elongation in (2.13). By finding a coordinate system  $(\mathbf{n}_1, \mathbf{n}_2, \mathbf{n}_3)$  such that the shear strains become zero the principal strains can be defined using

$$(\varepsilon_{ij} - \lambda\delta_{ij})n_j = 0 \quad (2.19)$$

where it becomes clear that  $\varepsilon_{ij} - \lambda\delta_{ij}$  can be written out as a  $3 \times 3$  matrix. To obtain a non-zero solution for  $n_j$  the determinant of this  $3 \times 3$  matrix must be equal to zero, that is to say

$$\det(\varepsilon_{ij} - \lambda\delta_{ij}) = 0 \quad (2.20)$$

This equation is known as the *characteristic equation* in which the eigenvalues  $\lambda_1, \lambda_2$  and  $\lambda_3$  determine the *principal strains*, as  $\lambda_1 = \varepsilon_1, \lambda_2 = \varepsilon_2$  and  $\lambda_3 = \varepsilon_3$  Ottosen and Ristinmaa (2005).

$$\varepsilon_{ij} = \begin{bmatrix} \varepsilon_1 & 0 & 0 \\ 0 & \varepsilon_2 & 0 \\ 0 & 0 & \varepsilon_3 \end{bmatrix} \quad (2.21)$$

### 2.2.2 Generic strain invariants

Expanding the expression in (2.20) one can write the *characteristic equation* in a more manageable form,

$$-\lambda^3 + \theta_1\lambda^2 - \theta_2\lambda + \theta_3 = 0 \quad (2.22)$$

where  $\theta_1, \theta_2, \theta_3$  denote the *Cauchy-strain invariants*

$$\begin{aligned} \theta_1 &= \varepsilon_{ii} \\ \theta_2 &= \frac{1}{2}(\varepsilon_{ii}\varepsilon_{jj} - \varepsilon_{ij}\varepsilon_{ji}) \end{aligned} \quad (2.23)$$

$$\theta_3 = \det(\varepsilon_{ij})$$

Furthermore there exists a more important series of invariants, called *generic strain invariants*. These generic invariants get their name from the systematic manner they are defined by

$$\begin{aligned}\tilde{I}_1 &= \varepsilon_{ii} = \varepsilon_1 + \varepsilon_2 + \varepsilon_3 \\ \tilde{I}_2 &= \frac{1}{2}\varepsilon_{ij}\varepsilon_{ji} = \frac{1}{2}(\varepsilon_1^2 + \varepsilon_2^2 + \varepsilon_3^2) \\ \tilde{I}_3 &= \frac{1}{3}\varepsilon_{ij}\varepsilon_{jk}\varepsilon_{ki} = \frac{1}{3}(\varepsilon_1^3 + \varepsilon_2^3 + \varepsilon_3^3)\end{aligned}\tag{2.24}$$

Finally it follows that a unique relation exists between the generic invariants and the Cauchy invariants (Ottosen and Ristinmaa; 2005)

$$\begin{aligned}\tilde{I}_1 &= \theta_1 \\ \tilde{I}_2 &= \frac{1}{2}\theta_1^2 - \theta_2 \\ \tilde{I}_3 &= \frac{1}{3}\theta_1^3 - \theta_1\theta_2 + \theta_3\end{aligned}\tag{2.25}$$

### 2.2.3 Strain deviator invariants

In similarity to how the generic strain invariants were formed from the strain tensor, one can form invariants from the *deviator strain tensor*.

$$e_{ij} = \varepsilon_{ij} - \frac{1}{3}\varepsilon_{kk}\delta_{ij}\tag{2.26}$$

Comparing the deviator strain tensor,  $e_{ij}$ , to the small strain tensor,  $\varepsilon_{ij}$ , it is clear that they are similar, the difference lies in the term  $\frac{1}{3}\varepsilon_{kk}\delta_{ij}$ , referred to as the *volumetric strain tensor*. In analogy with (2.24) the generic invariants of the deviator strain tensor can be formed as

$$\begin{aligned}\tilde{J}_1 &= e_{ii} = e_1 + e_2 + e_3 \\ \tilde{J}_2 &= \frac{1}{2}e_{ij}e_{ji} = \frac{1}{2}(e_1^2 + e_2^2 + e_3^2) \\ \tilde{J}_3 &= \frac{1}{3}e_{ij}e_{jk}e_{ki} = \frac{1}{3}(e_1^3 + e_2^3 + e_3^3)\end{aligned}\tag{2.27}$$

It is also possible to find a relation between the generic invariants of the deviator strain tensor,  $\tilde{J}_1, \tilde{J}_2, \tilde{J}_3$ , and the generic invariants of the strain tensor,  $\tilde{I}_1, \tilde{I}_2, \tilde{I}_3$ .

# 3 Stress

## 3.1 Stress tensor

In this chapter the stress expression will be explored, doing this it is suitable to start by studying a continuous body as shown in Figure 3.1. Imagine that two different forces act on the body, one force acting on the surface of the body (a force per unit area) and one body force (a force per unit volume). These forces will give rise to internal forces acting on all surfaces of the body both external and within the body (i.e. obtained from section of the body), see figure 3.1.

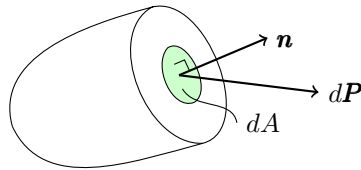


Figure 3.1: *Continuous body showing a section where a force  $d\mathbf{P}$  acts on the surface  $dA$ .*

By studying the incremental force vector  $d\mathbf{P}$ , see Figure 3.1, acting on the infinitesimal surface area  $dA$  with the normal unit vector  $\mathbf{n}$  directed out from its surface, the so called *traction vector*,  $\mathbf{t}$ , can be defined. This is done by the assumption that the ratio  $d\mathbf{P}/dA$  approaches the value  $\mathbf{t}$  as the surface  $dA$  approaches zero.

### 3.1. STRESS TENSOR

---

$$\mathbf{t} = \left( \frac{d\mathbf{P}}{dA} \right)_{dA \rightarrow 0} \quad \mathbf{t} = \begin{bmatrix} t_1 \\ t_2 \\ t_3 \end{bmatrix} \quad (3.1)$$

The components  $t_1$ ,  $t_2$  and  $t_3$  of the traction vector are pointing in the  $x_1$ -,  $x_2$ - and  $x_3$ - directions respectively and has the unit  $\text{N/m}^2$ . Since the traction vector is related to a surface with the normal unit vector  $\mathbf{n}$ , the value of  $\mathbf{t}$  can vary in a certain point depending on which section through the point one considers. To determine the traction vector for an arbitrary section through a specific point one can use the *stress tensor*.

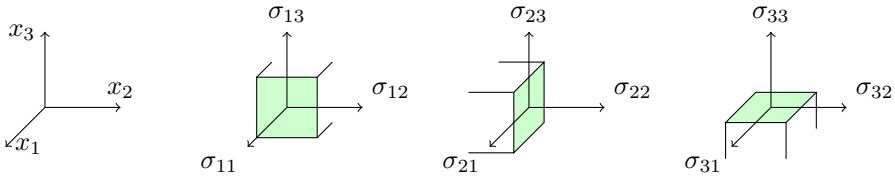


Figure 3.2: *The components of a stress tensor.*

To define the stress tensor, consider the three sections with the outer normal vector  $\mathbf{n}$  parallel to the  $x_1$ -,  $x_2$ - and  $x_3$ - axis through a point, see Figure 3.2. The corresponding traction vectors for these sections are denoted  $\mathbf{t}_1$ ,  $\mathbf{t}_2$  and  $\mathbf{t}_3$  with their  $x_1$ -,  $x_2$ - and  $x_3$ -components according to

$$\mathbf{t}_1 = \begin{bmatrix} \sigma_{11} \\ \sigma_{12} \\ \sigma_{13} \end{bmatrix} \quad \mathbf{t}_2 = \begin{bmatrix} \sigma_{21} \\ \sigma_{22} \\ \sigma_{23} \end{bmatrix} \quad \mathbf{t}_3 = \begin{bmatrix} \sigma_{31} \\ \sigma_{32} \\ \sigma_{33} \end{bmatrix} \quad (3.2)$$

The  $\sigma_{11}$ ,  $\sigma_{22}$ ,  $\sigma_{33}$  components are denoted *normal stresses* and  $\sigma_{12}$ ,  $\sigma_{13}$ ,  $\sigma_{21}$ ,  $\sigma_{23}$ ,  $\sigma_{31}$  and  $\sigma_{32}$  are called *shear stresses*. Further notice the notation in (3.2) where the first index of each component denotes the direction of the outer normal unit vector for its associated traction vector, i.e. all components  $\sigma_{1j}$  originate in the  $\mathbf{t}_1$  traction vector. The second index denotes the direction of the component, i.e. all  $\sigma_{i3}$  components are the  $x_3$ -components of their associated traction vector. Using

the traction vectors in (3.2) the *stress tensor* can be defined as

$$\sigma_{ij} = \begin{bmatrix} t_1^T \\ t_2^T \\ t_3^T \end{bmatrix} = \begin{bmatrix} \sigma_{11} & \sigma_{12} & \sigma_{13} \\ \sigma_{21} & \sigma_{22} & \sigma_{23} \\ \sigma_{31} & \sigma_{32} & \sigma_{33} \end{bmatrix} \quad (3.3)$$

It can be proven that the stress tensor is symmetric, (i.e.  $\sigma_{12} = \sigma_{21}$ ,  $\sigma_{13} = \sigma_{31}$ ,  $\sigma_{23} = \sigma_{32}$ ), and contains all the information that is needed to determine the traction vector,  $\mathbf{t}$ , for an arbitrary surface through a certain point.

$$t_i = \sigma_{ij}n_j \quad (3.4)$$

If the point is on the exterior surface of a body the equation describes a relation between the external force and the stress tensor. Equation (3.4) was first proven by Cauchy in 1822 and the equation is often called *Cauchy's formula*, (Ottosen and Ristinmaa; 2005).

## 3.2 Stress invariants

As for the strain tensor handled in the previous chapter there exists invariants to the stress tensor. In this section the invariants to the stress tensor will be discussed. As for the strain tensor the invariants to the stress tensor will not be derived in full and the reader is referred to other literature on the topic for further studies.

### 3.2.1 Principal stresses

Letting the normal stresses previously defined as  $\sigma_{11}, \sigma_{22}, \sigma_{33}$  be denoted  $\sigma_n$ , in other words  $\sigma_n = n_i t_i = n_i \sigma_{ij} n_j$ . In similarity the shear stresses, are denoted  $\tau_n$  and composed from  $\tau_n = m_i t_i = m_i \sigma_{ij} n_j$ . Figure 3.3 illustrates the direction of the normal- and shear stresses for an arbitrary element.

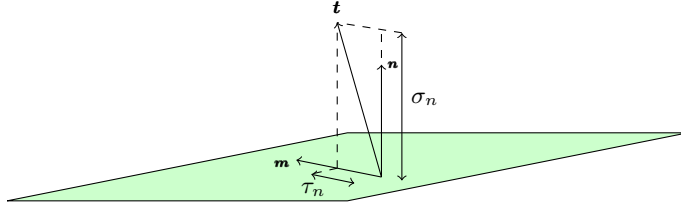


Figure 3.3: Normal and shear stress

For a case where the traction vector is parallel to the unit vector  $\mathbf{n}$  it is clear that

$$t_i = \lambda n_i = \sigma_n n_i \quad (3.5)$$

where  $\lambda$  is a constant of proportionality. From (3.5) an eigenvalue problem corresponding to (2.19), as derived for the strain case, can be determined as

$$(\sigma_{ij} - \lambda \delta_{ij}) n_j = 0 \quad (3.6)$$

In analogy to the strain case  $\sigma_{ij} - \lambda \delta_{ij}$  can be written out as a  $3 \times 3$  matrix and as for the strains, to obtain a non-zero solution for  $n_j$  the determinant of this  $3 \times 3$  matrix must be equal to zero. This leads to an equation corresponding to (2.20), the characteristic equation

$$\det(\sigma_{ij} - \lambda \delta_{ij}) = 0 \quad (3.7)$$

Corresponding to the case for strains, the eigenvalues  $\lambda_1$ ,  $\lambda_2$  and  $\lambda_3$  determine the *principal stresses* as  $\lambda_1 = \sigma_1$ ,  $\lambda_2 = \sigma_2$  and  $\lambda_3 = \sigma_3$  and their corresponding principal directions can then be determined from  $\mathbf{n}_i$ .

### 3.2.2 Generic stress invariants

In analogy to the strain case the *Cauchy-stress invariants* are defined as

$$\begin{aligned} \Theta_1 &= \sigma_{ii} \\ \Theta_2 &= \frac{1}{2}(\sigma_{ii}\sigma_{jj} - \sigma_{ij}\sigma_{ji}) \\ \Theta_3 &= \det(\sigma_{ij}) \end{aligned} \quad (3.8)$$

Furthermore just as for the strain case there exists a more important series of invariants, the *generic stress invariants*.

$$\begin{aligned}
 I_1 &= \sigma_{ii} = \sigma_1 + \sigma_2 + \sigma_3 \\
 I_2 &= \frac{1}{2}\sigma_{ij}\sigma_{ji} = \frac{1}{2}(\sigma_1^2 + \sigma_2^2 + \sigma_3^2) \\
 I_3 &= \frac{1}{3}\sigma_{ij}\sigma_{jk}\sigma_{ki} = \frac{1}{3}(\sigma_1^3 + \sigma_2^3 + \sigma_3^3)
 \end{aligned} \tag{3.9}$$

Also in analogy to (2.25) a unique relation exists between the generic invariants and the Cauchy invariants.

$$\begin{aligned}
 I_1 &= \Theta_1 \\
 I_2 &= \frac{1}{2}\Theta_1^2 - \Theta_2 \\
 I_3 &= \frac{1}{3}\Theta_1^3 - \Theta_1\Theta_2 + \Theta_3
 \end{aligned} \tag{3.10}$$

### 3.2.3 Deviator stress invariants

Just as for strains, one can form invariants from the *deviator stress tensor* given from

$$s_{ij} = \sigma_{ij} - \frac{1}{3}\sigma_{kk}\delta_{ij} \tag{3.11}$$

The term  $\frac{1}{3}\sigma_{kk}\delta_{ij}$  is referred to as the *hydrostatic stress tensor* and has great influence on the failure criteria for friction materials. In analogy with (3.9) the generic invariants of the deviator stress tensor can be formed as

$$\begin{aligned}
 J_1 &= s_{ii} = s_1 + s_2 + s_3 \\
 J_2 &= \frac{1}{2}s_{ij}s_{ji} = \frac{1}{2}(s_1^2 + s_2^2 + s_3^2) \\
 J_3 &= \frac{1}{3}s_{ij}s_{jk}s_{ki} = \frac{1}{3}(s_1^3 + s_2^3 + s_3^3)
 \end{aligned} \tag{3.12}$$

As for the case with strains it appears that it is possible to find a relation between the generic invariants of the deviator stress tensor,  $J_1, J_2, J_3$ , and the generic invariants of the stress tensor,  $I_1, I_2, I_3$ . Thus making it valid to use the  $J_2$  and  $J_3$  together with the  $I_1$  invariant will help to describe the material behaviors later on.

### 3.2. STRESS INVARIANTS

---

It is also essential to comprehend the meaning of an *octahedral plane*, as stresses are considered the octahedral plane refers to the plane that has a normal vector with an equal angle to the principal stress directions, see Figure 3.4 below.

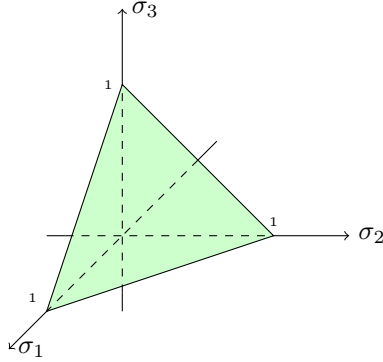


Figure 3.4: *Example of octahedral plane.*

There are two quantities that are related to this octahedral plane, the *octahedral normal stress*,  $\sigma_{oct}$ , and the *octahedral shear stress*,  $\tau_{oct}$ , which both act on the octahedral plane (Ottosen and Ristinmaa; 2005).

$$\sigma_{oct} = \frac{1}{3}I_1 \tag{3.13}$$

$$\tau_{oct} = \sqrt{\frac{2}{3}J_2}$$

Looking back at (3.11) it is clear that the hydrostatic stress is defined by the octahedral normal stress,  $\sigma_{oct}$ .

#### 3.2.4 The Lode angle, $\theta$

Another important invariant when discussing failure criteria for friction materials is the *Lode angle* often denoted  $\theta$  and named after Lode (1926), (Ottosen and Ristinmaa; 2005). The Lode angle is defined as

$$\cos 3\theta = \frac{3\sqrt{3}}{2} \frac{J_3}{J_2^{3/2}} \tag{3.14}$$

### 3.2.5 Mean pressure, $p$ , and the equivalent stress, $q$

Two invariants often used when defining material models for rocks, soils and ceramics are the *mean pressure*,  $p$ , and the *von Mises equivalent stress*,  $q$ , defined as.

$$p = \frac{1}{3}I_1 \tag{3.15}$$

$$q = \sqrt{3J_2} \tag{3.16}$$

## 3.3 Various states of stress

Finally it is important to have a good understanding of how the different states of stress presented in this chapter. Therefore some specific stress states are illustrated in Figure 3.5.

### 3.3. VARIOUS STATES OF STRESS

---

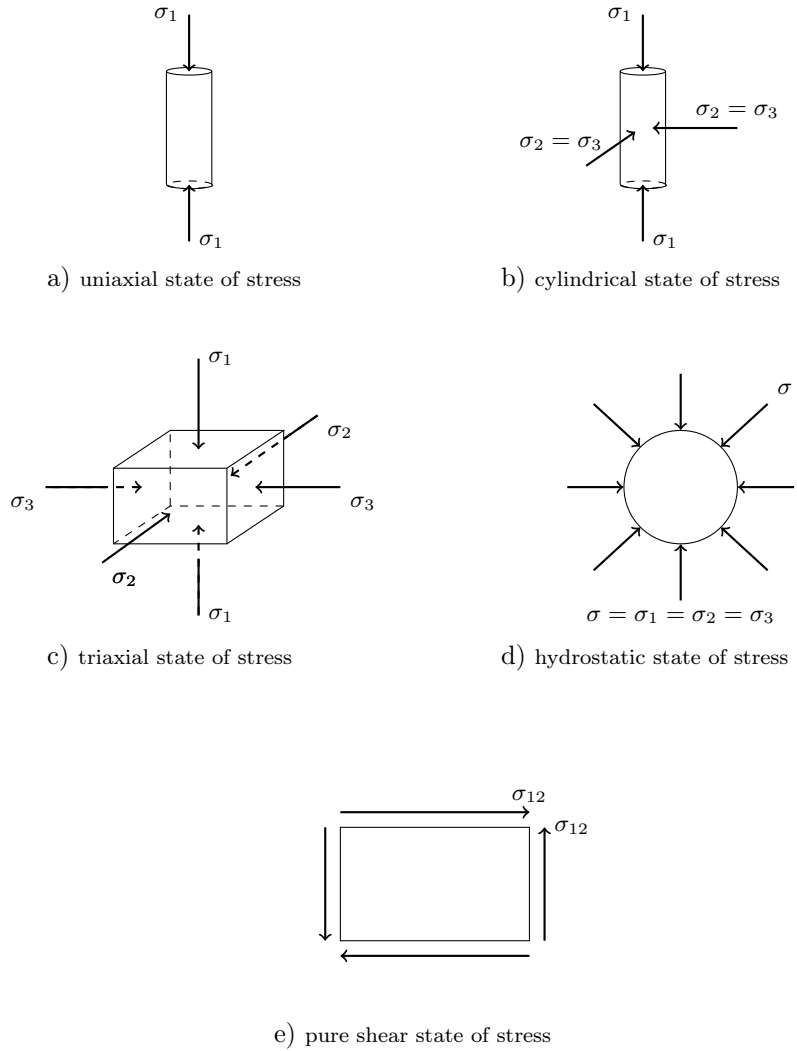


Figure 3.5: *Various states of stress.*

# 4 Constitutive relations

The stress and strain expressions have been established in the previous chapters. This chapter will handle the relation between these quantities. The relations between stresses and strains are called *constitutive relations* or *models* and are specific to each material. As constitutive relations for soils often are rather complicated this chapter will start out with presenting the most basic constitutive relation, followed by the more complex theory of plasticity. The chapter will round up with a presentation of some material models that are widely used when modeling soils.

## 4.1 Linear elasticity

Experimental observations have shown that many materials behave elastically up to a certain stress level and can therefore be handled as linear elastic. The simplest linear elastic relation is called *Hyper-elasticity*, i.e. the material elastic response is independent of the load history. For isotropic materials displaying hyper-elasticity the relation between stresses and strains is defined by two material properties, namely *Young's modulus*, also referred *elasticity modulus*, and *Poisson's ratio*, denoted  $E$  and  $\nu$  respectively. With the help of these properties a relation between the stress and strain tensor can be formed as a fourth-order elasticity tensor  $D_{ijkl} = D_{ijlk}$  called the *stiffness tensor*. Though it would be possible to form the stiffness tensor using Young's modulus and Poisson's ratio the expression becomes more manageable when using the *shear modulus*,  $G$ , and the *bulk modulus*,  $K$  defined as

$$G = \frac{E}{2(1 + \nu)} \tag{4.1}$$

$$K = \frac{E}{3(1 - 2\nu)} \quad (4.2)$$

A stress-strain relation can then be retained using these quantities as

$$\sigma_{ij} = 3K \left( \frac{1}{3} \varepsilon_{kk} \delta_{ij} \right) + 2G \left( \varepsilon_{ij} - \frac{1}{3} \varepsilon_{kk} \delta_{ij} \right)$$

or in a much useful manner using that  $\varepsilon_{ij} = \frac{1}{2}(\delta_{ik}\delta_{jl} + \delta_{il}\delta_{jk})\varepsilon_{kl}$

$$\sigma_{ij} = 2G \left[ \frac{1}{2}(\delta_{ik}\delta_{jl} + \delta_{il}\delta_{jk}) + \frac{\nu}{1 - 2\nu} \delta_{ij}\delta_{kl} \right] \varepsilon_{kl}$$

From this expression it is evident that the first part on the right-hand side can be recognized as the stiffness tensor, that is,

$$D_{ijkl} = 2G \left[ \frac{1}{2}(\delta_{ik}\delta_{jl} + \delta_{il}\delta_{jk}) + \frac{\nu}{1 - 2\nu} \delta_{ij}\delta_{kl} \right] \quad (4.3)$$

Using  $D_{ijkl}$  the constitutive relation between stresses and strains for a linear hyper-elastic material can then be written as

$$\sigma_{ij} = D_{ijkl}\varepsilon_{kl} \quad (4.4)$$

This equation can be recognized as *Hooke's generalized law* for isotropic elasticity and was in a uniaxial form suggested by Robert Hooke in 1676. As  $D_{ijkl}$  is an isotropic fourth-order tensor and  $\sigma_{ij}$  and  $\varepsilon_{ij}$  are second order tensors, it is possible to form an inverted expression of (4.4) to determine the strains using that  $C = D^{-1}$ .

$$\varepsilon_{ij} = C_{ijkl}\sigma_{kl} \quad (4.5)$$

where  $C_{ijkl}$  is termed the *elastic isotropic flexibility tensor*, defined as (Ottosen and Ristinmaa; 2005).

$$C_{ijkl} = \frac{1}{2G} \left[ \frac{1}{2}(\delta_{ik}\delta_{jl} + \delta_{il}\delta_{jk}) - \frac{\nu}{1 + \nu} \delta_{ij}\delta_{kl} \right] \quad (4.6)$$

## 4.2 Plasticity theory

The linear elastic model presented in the previous is generally considered too crude to model the essential features of soil behavior, therefore an introduction to the *plasticity theory* is necessary. The plasticity theory is concerned with materials that after a load-unload cycle retain a part of the deformation, i.e. do

not return to its original configuration after unloading. This behavior is due to the plastic strains  $\varepsilon_{ij}^p$  developed in the material as the stress state exceeds the material *initial yield stress*  $\sigma_{y0}$ . This phenomenon is illustrated in the uniaxial stress-strain curve in Figure 4.1

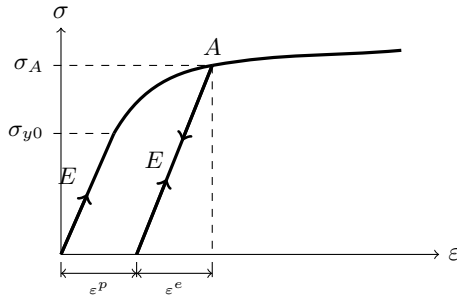


Figure 4.1: *Typical stress-strain curve for metal under simple tension.*

Until the stress state reaches  $\sigma_{y0}$  the stress strain behavior can be described with linear elasticity, i.e. (4.4). When the stress state exceeds  $\sigma_{y0}$  the total strains  $\varepsilon_{ij}$  will be given from the sum of the elastic and plastic strains

$$\varepsilon_{ij} = \varepsilon_{ij}^e + \varepsilon_{ij}^p \quad (4.7)$$

This graphical interpretation is illustrated in Figure 4.1.

Before going further into plastic behavior, it is appropriate to elaborate on the stress level where yielding first occurs, i.e. the initial yield stress for the uniaxial case demonstrated above (Ottosen and Ristinmaa; 2005).

### 4.2.1 Yield criteria

A *yield criterion* may be defined as the limitation of elastic deformations expressed by a combination of stresses. As illustrated earlier, for the one-dimensional case the initial yield stress  $\sigma_{y0}$ , can be described by a uniaxial compressive or tensile stress and relatively easy to comprehend. For the multi-axial stress state though, it becomes more complicated to determine the initial yield stress or rather *initial yield surface*. The yield expression for the multi-axial case often involves all terms of the stress tensor and is conveniently expressed as a scalar function,  $F$ . For isotropic materials the initial yield function is dependent only on the stress tensor and may be written as

$$F(\sigma_{ij}) = F(\sigma_{11}, \sigma_{22}, \sigma_{33}, \sigma_{12}, \sigma_{23}, \sigma_{13}) \quad (4.8)$$

The mathematical expression describing this initial yield surface has to be established from experimental observations. One simplification done concerning soil is that it will be handled as an isotropic material, which leads to that the material does not have any preferred directions, therefore the initial yield criterion can be expressed with the principal stresses, or rather with help of the stress invariants presented in Chapter 3

$$F(\sigma_{ij}) = F(I_1, J_2, \cos 3\theta) \quad (4.9)$$

One reason that it is beneficial to use the stress invariants instead of the principal stresses to define the yield criterion is that the eigenvalue problem presented by the *characteristic equation* in (3.8) can be avoided. Another advantage is that the *hydrostatic stress*,  $I_1/3$ , is separated from the deviator stresses in  $J_2$  and  $\cos 3\theta$ , this has a great significance for metals where experimental studies have shown that the influence of hydrostatic stress has little impact on the plastic deformations (Desai and Siriwardane; 1984).

Furthermore, it is possible to obtain useful geometrical interpretations from the invariants  $I_1, J_2$  and  $\cos 3\theta$ , as will be described. Starting by establishing the *deviatoric plane* as the three-dimensional stress space with the principal directions as the coordinate axes. As shown in Figure 4.2a the hydrostatic stress creates the space diagonal to the deviatoric plane. Viewing the deviatoric plane in the direction of the hydrostatic axis, the projection creates a widely used graphical interpretation of the yield criterion. This projection of the deviatoric plane is often referred to as the  $\pi$ -plane which is illustrated in Figure 4.2b.

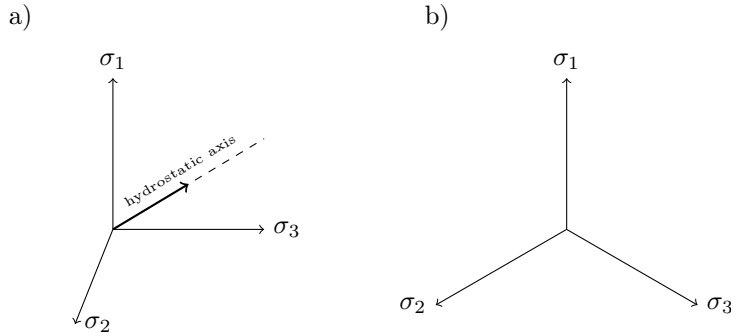


Figure 4.2: a) *The hydrostatic axis in the principal stress space*, b) *The deviatoric plane often called the  $\pi$ -plane, i.e. the principal stress space viewed from the direction of the hydrostatic axis.*

Forming a possible shape of yield surface in the  $\pi$ -plane according to Figure 4.3a

it can be shown that a yield criterion is symmetric around  $\theta = 60^\circ$ ,  $\theta = 180^\circ$  and  $\theta = 300^\circ$ , where  $\theta$  in the graphics is the *Lode angle* presented in Chapter 3. It is therefore possible to fully determine the yield criterion in the deviatoric plane from the curve  $0^\circ \leq \theta \leq 60^\circ$ . One more geometrical interpretation that is of importance when discussing material models is the *meridians* of the initial yield surface. The meridians are the curves where the value of  $\theta$  is constant, see example in Figure 4.3b. The meridians are commonly presented in the so-called *meridian plane*, with a  $I_1, \sqrt{J_2}$ -coordinate system illustrated in Figure 4.3b (Ottosen and Ristinmaa; 2005).

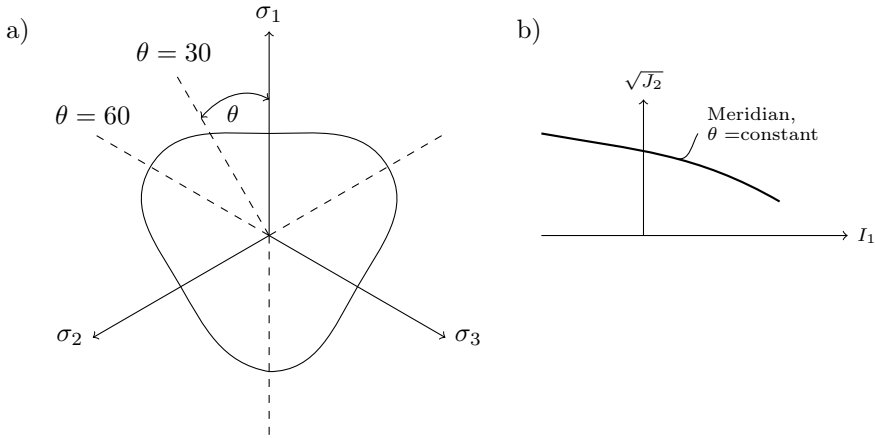


Figure 4.3: Projection of the Mohr-Coulomb criterion on the deviator plane.

There are three meridians of specific interest, these are the *tensile meridian*,

$$\sigma_1 > \sigma_2 = \sigma_3 \quad \text{i.e. } \theta = 0^\circ \quad (4.10)$$

the *compressive meridian*,

$$\sigma_1 = \sigma_2 > \sigma_3 \quad \text{i.e. } \theta = 60^\circ \quad (4.11)$$

and the *shear meridian*.

$$\sigma_1 > \sigma_2 = \frac{\sigma_1 + \sigma_3}{2} > \sigma_3 \quad \text{i.e. } \theta = 30^\circ \quad (4.12)$$

As this report focuses on geotechnical materials it might be time to evaluate some material failure characteristics for soils and friction materials before going into post yield behaviors. One important aspect of the yield surface when talking

about friction materials is that they are characterized by smooth stress-strain curves, making it difficult to establish a well defined initial yield stress. Also in contrast to metals and non-friction materials whose yielding or plastic behavior has shown an independence to the hydrostatic stress, experimental tests on friction materials show that their strength has a strong dependence of the hydrostatic stress, i.e. the strength of soils often increases with the hydrostatic stress. Experimental results have also proven that for most friction materials the yield surface takes a convex form in the deviatoric plane, which is illustrated in Figure 4.3a (Ottosen and Ristinmaa; 2005).

### 4.2.2 Post-yield behavior

In the previous it has been established that the plastic strains start to take place as the stress state reaches the initial yield criterion. Before discussing the detail of the plasticity theory some idealized stress-strain behaviors for the uniaxial case are illustrated in Figure 4.4 below.

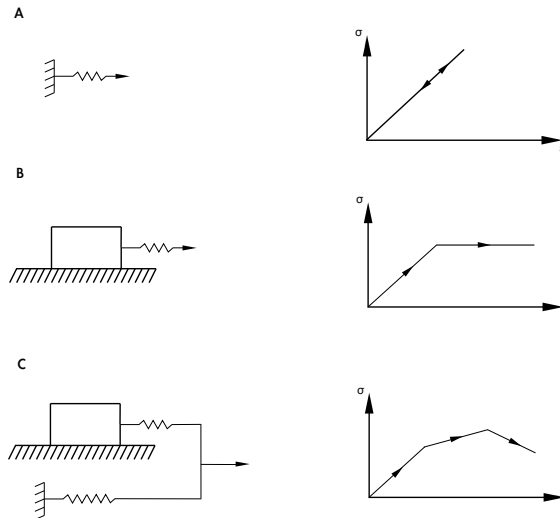


Figure 4.4: Different idealized stress-strain models, A - Linear elasticity, B - Elastic perfectly plastic, and C - Elastic, linear hardening/softening (Desai and Siriwardane; 1984).

One characteristic behavior of a material that suffers irreversible deformations,  $\epsilon_p$ , appears if a load-reload cycle as the one shown in Figure 4.5 is considered. It

becomes evident that the reloading path differs from the original loading path, which implies that the material behavior is no longer only determined from current stress state but rather said to be history dependent, i.e. it can only be determined by an integration of the load history. To help visualizing this effect a study of points  $D$ ,  $E$  and  $F$  in Figure 4.5 can be done, where it is obvious that the strains are equal at different stress levels.

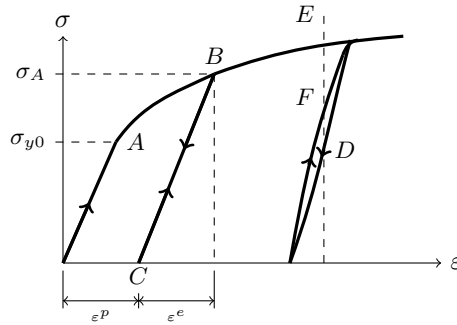


Figure 4.5: Load-reload cycle for a uniaxial stress-strain curve.

Furthermore it can be realized from a study of Figure 4.5 that yielding will not occur at the initial yielding  $\sigma_{y0}$  but at  $\sigma_A$  when reloaded from point  $C$ , this stress-strain response is called *hardening* behavior and will be discussed more in detail shortly. First it should be mentioned that due to the dependence of the load history demonstrated in Figure 4.5, constitutive models for plasticity are written in an incremental form with their corresponding incremental plastic strains  $\dot{\varepsilon}_{ij}^p$ . This indicates a time-dependence even though time does not influence the material response. However  $\varepsilon_{ij}^p$  is used instead of  $d\varepsilon_{ij}^p$  plainly to simplify the notation (Ottosen and Ristinmaa; 2005).

### 4.2.3 Hardening rules

As mentioned earlier the *hardening behavior* or *hardening rule* describes how the yield surface changes with the plastic load. In the following, mathematical expressions for how the hardening for the idealized plastic behaviors illustrated in Figure 4.4 will be presented. First, however, the parameters regulating this hardening behavior will be established, this can be done stating that the yield surface load dependency can be expressed with the *current yield surface*

$$f(\sigma_{ij}, K_\alpha) = 0 \quad \text{where} \quad K_\alpha = K_1, K_2, \dots, K_n \quad (4.13)$$

where  $K_\alpha$  denotes the so-called *hardening parameters* describing the changes in shape, size and position of the yield surface. However, until plastic deformation takes place the hardening parameters are per definition zero, i.e. the current yield surface coincides with the initial yield surface.

$$f(\sigma_{ij}, 0) = F(\sigma_{ij}) \quad (4.14)$$

It was stated earlier that the current yield surface depends on the plastic load history. In the equations this appears as the *internal variable*,  $\kappa_\beta$ . The internal variable can be seen as a memory of the plastic loading history, and an assumption that the hardening parameter can be written as a function of  $\kappa_\alpha$  can be made (Ottosen and Ristinmaa; 2005).

$$K_\alpha = K_\alpha(\kappa_\beta) \quad \text{where} \quad \kappa_\beta = \kappa_1, \kappa_2, \dots, \kappa_n \quad (4.15)$$

Using the incremental notation, the hardening behavior will be given from

$$\dot{K}_\alpha = \frac{\partial K_\alpha}{\partial \kappa_\beta} \dot{\kappa}_\beta \quad (4.16)$$

As the internal variable describes the plastic load history, it becomes obvious that for *elastic behavior*

$$\dot{K}_\alpha = \dot{\kappa}_\beta = 0 \quad (4.17)$$

Having discussed the variables used to describe hardening, some important attributes of the different hardening rules will be reviewed in the following, starting with *ideal plasticity*. For ideal plasticity the yield surface remains fixed in the stress space, illustrated in Figure 4.6.

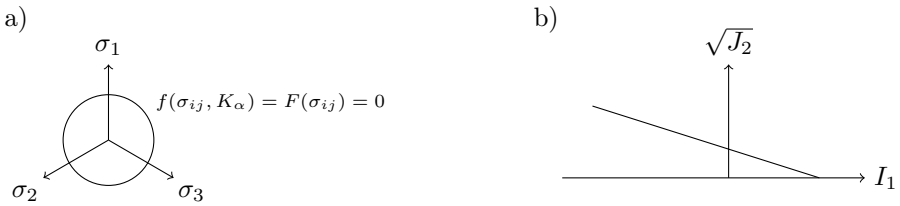


Figure 4.6: a) A principal yield surface in the stress space during plastic deformation for ideal plasticity, b) The yield surface in the meridian plane.

What is more, the current yield surface will coincide with the initial yield surface, which mathematically can be described with

$$f(\sigma_{ij}, K_\alpha) = F(\sigma_{ij}) = 0 \quad (4.18)$$

For a material that shows *isotropic hardening*, on the other hand, the yield surface changes in size while showing a consistent shape and position, these characteristics are illustrated in Figure 4.7.

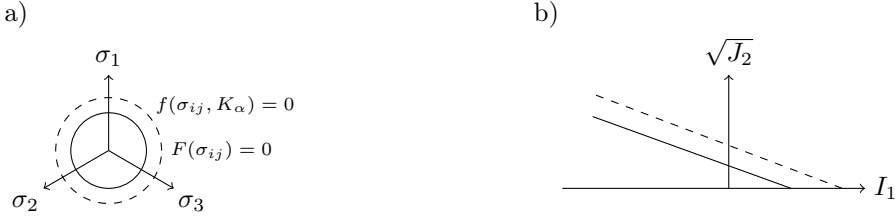


Figure 4.7: a) A principal yield surface in the stress space during plastic deformations for isotropic hardening, b) The change in yield surface in the meridian plane.

The change of size of the yield surface due to plastic loading is described with the hardening parameter,  $K_\alpha$  introduced above, hence the mathematical expression for isotropic hardening is obtained from

$$f(\sigma_{ij}, K_\alpha) = F(\sigma_{ij}) - K = 0 \quad (4.19)$$

The next hardening rule to be handled is called *kinematic hardening*, as the name suggests it holds that for kinematic hardening the yield surface will move during plastic deformation while the size and shape remains constant, this can be illustrated as a rigid body movement in the stress space.

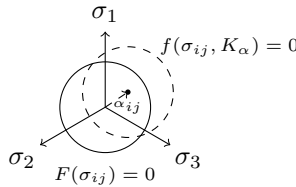


Figure 4.8: A principal yield surface in the stress space during plastic deformation for kinematic hardening.

In Figure 4.8  $\alpha_{ij}$  is a tensor describing the center of the yield surface, i.e.  $\alpha_{ij} = 0$  until plastic deformations take place. The kinematic hardening rule is mathe-

matically described with

$$f(\sigma_{ij}, K_\alpha) = F(\sigma_{ij} - \alpha_{ij}) = 0 \quad (4.20)$$

The last hardening rule is called *mixed hardening* and is a combination of isotropic hardening and kinematic hardening. For mixed hardening it yields that size and position of the yield surface vary with the plastic deformation while the shape of the yield surface remains consistent. These features can be illustrated in the stress space according to Figure 4.9

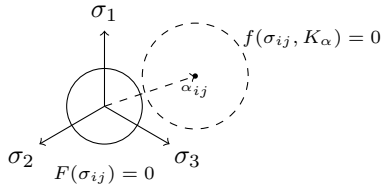


Figure 4.9: A principal yield surface in the stress space during plastic deformation for mixed hardening.

The mathematical expression for the mixed hardening rule will then be given from.

$$f(\sigma_{ij}, K_\alpha) = F(\sigma_{ij} - \alpha_{ij}) - K = 0 \quad (4.21)$$

Furthermore it should be mentioned that the isotropic hardening rule is common to use when the loading only increases, i.e. no unloading occurs. Whereas the kinematic hardening rule is adopted when cyclic loadings are studied (Ottosen and Ristinmaa; 2005).

#### 4.2.4 Flow rule

As the concept of hardening rules have been introduced one of the cornerstones in the plasticity theory is established. However, before a stress-strain relation can be established there are a few more building blocks that need to be discussed, first out is the so-called *flow rule*. The theory was first established in the 19th century and often called the *Lévy-von Mises equation*, the theory forms a relation between the total strains and the deviatoric stress as

$$\dot{\epsilon}_{ij} = \dot{\beta} s_{ij}; \quad \dot{\beta} \geq 0 \quad (4.22)$$

It was later established that for elastic-ideal plastic materials the plastic part of  $\varepsilon_{ij}$  could be determined from a similar expression,

$$\dot{\varepsilon}_{ij}^p = \dot{\beta} s_{ij}; \quad \dot{\beta} \geq 0 \quad (4.23)$$

This constitutive relation for  $\varepsilon_{ij}$  is called the *flow rule*. This original flow rule assumes that the material is incompressible under plastic flow or yielding, i.e. that the volumetric strain tensor  $\varepsilon_{ii}^p/3$  is equal to zero. This however is generally not true for geological materials (Desai and Siriwardane; 1984). As this report is concerned with friction materials, the Drucker-Prager yield criterion with the mixed hardening rule will be used to illustrate the flow rule when the volumetric strains play a part. The Drucker-Prager yield criterion will be discussed in more detail shortly and for now it is only stated that the Drucker-Prager yield criterion for mixed hardening is given from

$$f(\sigma_{ij}, K) = \sqrt{J_2} + \alpha I_1 - \sigma_y(\kappa); \quad f(\sigma_{ij}, K) = 0 \quad (4.24)$$

where  $\sigma_y(\kappa) = \sigma_{y0} + K(\kappa)$  and  $\sigma_{y0}$  the initial yield stress. Differentiating (4.24) one acquires

$$\frac{\partial f}{\partial \sigma_{ij}} = \alpha \delta_{ij} + \frac{s_{ij}}{2\sqrt{J_2}} \quad (4.25)$$

Combining the equation above with (4.22) an expression to determine the direction of the plastic strains can be obtained,

$$\dot{\varepsilon}_{ij}^p = \dot{\lambda} \frac{\partial f}{\partial \sigma_{ij}}; \quad \dot{\lambda} \geq 0 \quad (4.26)$$

Where  $\dot{\lambda}$  is the so-called *plastic multiplier* which regulates the magnitude of the plastic strains and is specific for the material model used. The plastic multiplier will be discussed more shortly, however it is concluded that for this case the plastic multiplier can be determined from

$$\dot{\lambda} = \left( \frac{s_{ij}}{\alpha \delta_{ij}} + 2\sqrt{J_2} \right) \dot{\beta} \quad (4.27)$$

Until the stress state reaches the yield surface, that is while  $f < 0$ , the term  $\frac{\partial f}{\partial \sigma_{ij}}$  can be seen as the normal to the yield surface  $f = 0$ , this is illustrated in Figure 4.10.

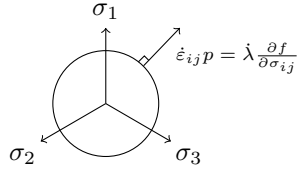


Figure 4.10: Normality of the incremental plastic strains.

As the normal to the yield surface is given from the *flow rule* in (4.27), the yield surface  $f$  can then be seen as a potential function for the incremental plastic strains. The flow rule can be given in a more general manner as

$$\dot{\epsilon}_{ij}^p = \dot{\lambda} \frac{\partial g}{\partial \sigma_{ij}}; \quad \dot{\lambda} \geq 0 \quad (4.28)$$

where  $g$  represents a non-specific *potential function*, that can take other forms than the yield surface  $f$ . The potential function,  $g$ , is in general determined with the same quantities as the yield surface, that is

$$g(\sigma_{ij}, K) = 0 \quad (4.29)$$

If  $g = f$  the flow rule is said to be *associated* and will simplify the plasticity theory. This *associated flow rule* has shown good numerical results compared to material testings of metals and non-friction materials, however for friction materials, experimental and numerical results have proven to diverge when the associated flow rule has been used, (Ottosen and Ristinmaa; 2005). Therefore a potential function, not equal to the yield surface is used when calculating soil behavior, i.e.  $g \neq f$ . The flow rule is then called the *non-associated flow rule* which is hence of special interest for this report.

### The consistency relation

The general flow rule and how the gradient  $\partial g / \partial \sigma_{ij}$  describes the direction of the plastic strains has now been established. It was also mentioned that  $\dot{\lambda}$  determines the magnitude of the plastic strains, which will be investigated more thorough in the following. Starting by recalling that when plastic loading occurs the yield surface will change according to the chosen hardening rule. Also remembering that the stress state per definition will be located on the yield surface, it is not improbable that, as plastic loading takes place, the current stress state will always be located on the current yield surface, i.e. (4.13), (Ottosen and Ristinmaa;

2005).

$$f(\sigma_{ij}, K_\alpha) = 0$$

This variation of the stress state so that it remains on the yield surface during plastic loading is governed by the variation of the hardening parameters  $K_\alpha$ , which is represented in the so-called *consistency relation*

$$\frac{\partial f}{\partial \sigma_{ij}} \dot{\sigma}_{ij} + \frac{\partial f}{\partial K_\alpha} \dot{K}_\alpha = 0 \quad (4.30)$$

As described earlier the hardening parameters  $K_\alpha$  are in turn dependent on the internal variables  $\kappa_\alpha$ . It is important to acknowledge that the relation between  $K_\alpha$  and  $\kappa_\alpha$  is established for the specific material properties of interest. However it turns out that it is possible to express this in a more general manner by introducing the *evolution functions*  $k_\alpha$ . This is done by first inserting the internal variable into (4.30), obtaining,

$$\frac{\partial f}{\partial \sigma_{ij}} \dot{\sigma}_{ij} + \frac{\partial f}{\partial K_\alpha} \frac{\partial K_\alpha}{\partial \kappa_\beta} \dot{\kappa}_\beta = 0 \quad (4.31)$$

Introducing  $k_\alpha$  as variables describing how  $\kappa_\alpha$  evolves with the plastic deformation the *evolution laws* can be established accordingly,

$$\dot{\kappa}_\alpha = \dot{\lambda} k_\alpha(\sigma_{ij}, K_\beta) \quad (4.32)$$

To scrutinize more on the evolution functions,  $k_\alpha$  and evolution laws, the reader is referred to other literature. That  $\dot{\lambda}$  is a part of the internal variable is not unexpected as it was earlier mentioned that  $\dot{\lambda}$  controls the magnitude of  $\dot{\epsilon}_{ij}^p$ , see (4.28). Moreover it follows that no plastic strains will develop when  $\dot{\lambda} = 0$  and that the internal variables will remain unchanged, (Ottosen and Ristinmaa; 2005).

Now using the previously derived parts of the plasticity theory a new quantity can be established, namely the plastic modulus,  $H$ . The assembly is done step by step, starting by putting the evolution laws into the hardening parameters, (4.16),

$$\dot{K}_\alpha = \dot{\lambda} \frac{\partial K_\alpha}{\partial \kappa_\beta} k_\beta \quad (4.33)$$

Inserting (4.33) in the consistency relation, (4.30) the following expression is obtained,

$$\frac{\partial f}{\partial \sigma_{ij}} \dot{\sigma}_{ij} + \dot{\lambda} \frac{\partial f}{\partial K_\alpha} \frac{\partial K_\alpha}{\partial \kappa_\beta} k_\beta = 0 \quad (4.34)$$

The plastic modulus  $H$ , can now be formed to simplify the expression as

$$H = -\frac{\partial f}{\partial K_\alpha} \frac{\partial K_\alpha}{\partial \kappa_\beta} k_\beta \quad (4.35)$$

Using the plastic modulus the expression in (4.34) is simplified into

$$\frac{\partial f}{\partial \sigma_{ij}} \dot{\sigma}_{ij} - \dot{\lambda} H = 0 \quad (4.36)$$

When the generalized plastic modulus  $H$  is obtained and once the yield function  $f$  and the potential function  $g$  are known the plasticity formulation is complete. Combining (4.36) and the flow rule established in (4.29)  $\dot{\epsilon}_{ij}^p$  is obtained from

$$\dot{\epsilon}_{ij}^p = \frac{1}{H} \left( \frac{\partial f}{\partial \sigma_{kl}} \dot{\sigma}_{kl} \right) \frac{\partial g}{\partial \sigma_{ij}} \quad (4.37)$$

### 4.2.5 Generalized stress and strain relation

As all parts of the plasticity theory now are known it is time to assemble these parts into a more general stress-strain relation. The plastic part of the strain tensor,  $\dot{\epsilon}_{ij}^p$ , established in (4.36) is determined from the current stress state, i.e. such a stress-strain relation is said to be stress driven. However a strain driven relation is often preferred, therefore, a strain driven form of the stress-strain relation will be derived in the following, starting by establishing that the total incremental strain can be obtained from

$$\dot{\epsilon}_{ij} = \dot{\epsilon}_{ij}^e + \dot{\epsilon}_{ij}^p \quad (4.38)$$

Using this expression Hooke's law, given in (4.4), can then be written as

$$\dot{\sigma}_{ij} = D_{ijkl} (\dot{\epsilon}_{kl} - \dot{\epsilon}_{kl}^p) \quad (4.39)$$

When the flow rule from equation (4.28) is inserted the expression changes into

$$\dot{\sigma}_{ij} = D_{ijkl} \dot{\epsilon}_{kl} - \dot{\lambda} D_{ijst} \frac{\partial g}{\partial \sigma_{st}} \quad (4.40)$$

Multiplication with  $\partial f / \partial \sigma_{ij}$  and using (4.34) makes it possible to form an expression to determine  $\dot{\lambda}$ , as

$$\dot{\lambda} = \frac{1}{A} \frac{\partial f}{\partial \sigma_{ij}} D_{ijkl} \dot{\epsilon}_{kl}; \quad \dot{\lambda} \geq 0 \quad (4.41)$$

Where  $A$  is defined by

$$A = H + \frac{\partial f}{\partial \sigma_{ij}} D_{ijkl} \frac{\partial g}{\partial \sigma_{kl}}; \quad A > 0 \quad (4.42)$$

Inserting the expression for  $\dot{\lambda}$  into the flow rule (4.28), it turns out that the plastic part of the strain tensor can be established when the total strains are known

$$\dot{\epsilon}_{ij}^p = \frac{1}{A} \left( \frac{\partial f}{\partial \sigma_{kl}} D_{klmn} \dot{\epsilon}_{mn} \right) \frac{\partial g}{\partial \sigma_{ij}} \quad (4.43)$$

This implies that if the total strain rates are known, the total stress rates can be determined from

$$\dot{\sigma}_{ij} = D_{ijkl}^{ep} \dot{\epsilon}_{kl} \quad (4.44)$$

The *elasto-plastic stiffness tensor*,  $D_{ijkl}^{ep}$ , which determines the current *tangential stiffness* of the material is defined as

$$D_{ijkl}^{ep} = D_{ijkl} + \frac{1}{A} D_{ijst} \frac{\partial g}{\partial \sigma_{st}} \frac{\partial f}{\partial \sigma_{mn}} D_{mnkl} \quad (4.45)$$

The expression in (4.44) is the sought general form of the stress-strain relation. It was first established by Hill in 1958 for associated plasticity and later in 1966 by Mroz for general non-associated plasticity (Ottosen and Ristinmaa; 2005). There are a few properties of the elasto-plastic stiffness tensor worth emphasizing, foremost it can be observed that  $D_{ijkl}^{ep}$  does not depend on either  $\dot{\sigma}_{ij}$  or  $\dot{\epsilon}_{ij}$  which results in that (4.44) is incrementally linear. Furthermore  $D_{ijkl}^{ep}$  shows similar symmetric properties as the stiffness tensor from (4.3), that is

$$D_{ijkl}^{ep} = D_{jikl}^{ep} \quad (4.46)$$

$$D_{ijkl}^{ep} = D_{ijlk}^{ep}$$

For associated plasticity it also yields that  $D_{ijkl}^{ep} = D_{klij}^{ep}$ , which does not hold for non-associated plasticity, i.e.  $D_{ijkl}^{ep} \neq D_{klij}^{ep}$  for non-associated plasticity. For numerical calculations using nonlinear finite element method it is of importance that (4.44) can be written on matrix form,

$$\dot{\boldsymbol{\sigma}} = \mathbf{D}^{ep} \dot{\boldsymbol{\epsilon}} \quad (4.47)$$

where it in compliance to previously discussed symmetric properties may be noticed that for associated plasticity  $\mathbf{D}^{ep} = \mathbf{D}^{epT}$  whereas for non-associated plasticity  $\mathbf{D}^{ep} \neq \mathbf{D}^{epT}$ .

### 4.2.6 Plane strain

When performing computational calculation on geotechnical problems it is often preferable to reduce a three-dimensional problem to two dimensions. This simplification of a three-dimensional problem results in reduced computational time whilst still giving satisfying results. For geotechnical applications the two-dimensional generalization used is commonly *plane strain*, i.e. no deformation is assumed out of plane. As this simplification is used for the calculations performed in this report, it is suitable to derive the strain driven generalized plasticity equation also for the case of plane strain. Letting the plane of interest be described by  $x_1x_2$ -coordinates, then the plane strain is characterized by

$$\dot{\epsilon}_{13} = \dot{\epsilon}_{23} = \dot{\epsilon}_{33} = 0 \quad (4.48)$$

As the plane strain is a two-dimensional problem and as the same notation is wanted Greek characters will be used to indicate the values 1, 2, while Latin characters denote values 1, 2 and 3. Using this notation the in-plane stress-strain relation is given from

$$\dot{\sigma}_{\alpha\beta} = D_{\alpha\beta\gamma\delta}^{ep} \dot{\epsilon}_{\gamma\delta} \quad (4.49)$$

where the elasto-plastic stiffness tensor is given from

$$D_{\alpha\beta\gamma\delta}^{ep} = D_{\alpha\beta\gamma\delta} + \frac{1}{A} D_{\alpha\beta st} \frac{\partial g}{\partial \sigma_{st}} \frac{\partial f}{\partial \sigma_{mn}} D_{mn\gamma\delta} \quad (4.50)$$

The parameter  $A$  is as earlier given from,

$$A = H + \frac{\partial f}{\partial \sigma_{ij}} D_{ijkl} \frac{\partial g}{\partial \sigma_{kl}}; \quad A > 0 \quad (4.51)$$

It is important to point out that though the strains out-of-plane are zero it is not generally so for the out-of-plane stress components,  $\dot{\sigma}_{13}$ ,  $\dot{\sigma}_{23}$  and  $\dot{\sigma}_{33}$ . These stress components need to be determined separately since they, in general, are part of the expression for the yield surface. The out-of-plane stress state can be established from

$$\dot{\sigma}_{i3} = D_{i3\gamma\delta}^{ep} \dot{\epsilon}_{\gamma\delta} \quad (4.52)$$

Furthermore the out-of-plane plastic strain components  $\dot{\epsilon}_{13}^p$ ,  $\dot{\epsilon}_{23}^p$  and  $\dot{\epsilon}_{33}^p$  need to be established as they can enter the expression for internal variable  $\kappa_\alpha$ . This can be done using

$$\dot{\epsilon}_{i3}^p = \dot{\lambda} \frac{\partial g}{\partial \sigma_{i3}}; \quad \text{where} \quad \dot{\lambda} = \frac{1}{A} \frac{\partial f}{\partial \sigma_{kl}} D_{kl\gamma\delta} \dot{\epsilon}_{\gamma\delta} \quad (4.53)$$

# 5 Soil behavior

In the previous chapters the general concepts of stress and strain have been reviewed as well as the general stress-strain relations for the plasticity theory. In this chapter the mechanical behavior of soil will be explored, reviewing the internal material properties that affect the stress-strain relation. As earth materials are complex and depend on several material parameters a thorough review would be all to comprehensive for this report. Instead this chapter mainly intends to serve as an overview for some of the material parameters in soil that have great influence on numerical modeling of friction materials. The chapter will be finished by presenting two of the most widely used material models when simulating soil behavior, namely the Mohr-Coulomb criterion and the Drucker-Prager criterion.

## 5.1 Soil strength

All aspects of soil stability, i.e. bearing capacity, supporting capacity of deep foundations or slope stability, are dependent on the soil strength, i.e the stress at material failure. The relation between stress and deformation, either direct or over time, is therefore of interest to all constructions where ground movement has to be considered. The amount of effort that is required to displace a group of particles in a soil influences the compressibility, deformation and strength properties of the soil. However, the reluctance to deform in a soil differs to most other engineering materials, where the deformational resistance is provided from chemical forces binding atoms, molecules and particles together (Mitchell and Soga; 2005). These forces do exist in soils as well but do not have a great influence on the compression and strength properties. Instead the soil strength properties depend primarily on gravity through self weight and on stresses applied to the soil.

### 5.1.1 Effective Stress

A soil generally consists of three material states, rock particles, fluid and gas. The structure of the soil is generally formed by the rock particles and the voids in-between the particles will be filled with fluid and gas, commonly water and air. The structure of a soil is of great importance as the particle structure of a soil can carry both normal and shear stress, whereas the fluid and gas phases can carry normal stress but not shear stress (Mitchell and Soga; 2005). If the voids in a soil are filled with water the stresses at any point consists of two parts, one part,  $u$ , that acts in the water and one part carried by the structure of the soil. The stress balance can then be described with the expression

$$\sigma' = \sigma - u \quad (5.1)$$

The term  $\sigma'$  is called *effective stress* and is fundamental to soil mechanics. The principles of effective stress asserts that the effective stress controls the stress-strain, volume change and strength properties of a soil independent of the pore pressure (Mitchell and Soga; 2005). As both the total stress,  $\sigma$ , and the pore water pressure,  $u$ , can be established from measurements or computed using external and body forces, it is always possible to establish the effective stress with (5.1). As mentioned above, the pore water pressure cannot carry shear stress, therefore the effective stress for all the stress components will be established from

$$\sigma'_{ij} = \begin{bmatrix} \sigma_{11} - u & \tau_{12} & \tau_{13} \\ \tau_{21} & \sigma_{22} - u & \tau_{23} \\ \tau_{31} & \tau_{32} & \sigma_{33} - u \end{bmatrix} \quad (5.2)$$

where it can be noted that  $\tau$  is used to denote the shear stresses that in Chapter 3 was denoted by  $\sigma$ , i.e.  $\tau_{12} = \sigma_{12}$ ,  $\tau_{13} = \sigma_{13}$  and  $\tau_{23} = \sigma_{23}$ .

### 5.1.2 Stress-strain relation in soil

Most stress-strain relations and strength properties of soils are mathematical equations based on empirical testings (Mitchell and Soga; 2005). The most widely used material relation for soils is the *Mohr-Coulomb* equation, which states

$$|\tau_f| = c - \sigma \tan \phi \quad (5.3)$$

or using effective material parameters,

$$|\tau_f| = c' - \sigma' \tan \phi' \quad (5.4)$$

where  $\tau_f$  is the shear stress at material failure on the *failure* or *slip plane*, see Figure 5.1. The parameter,  $\sigma$ , denotes the normal stress on the shear plane,  $c$ , denotes the intercept for  $\sigma = 0$ , usually mentioned as the material *cohesion* and where  $\phi$  denotes the slope and often called *internal friction angle*.

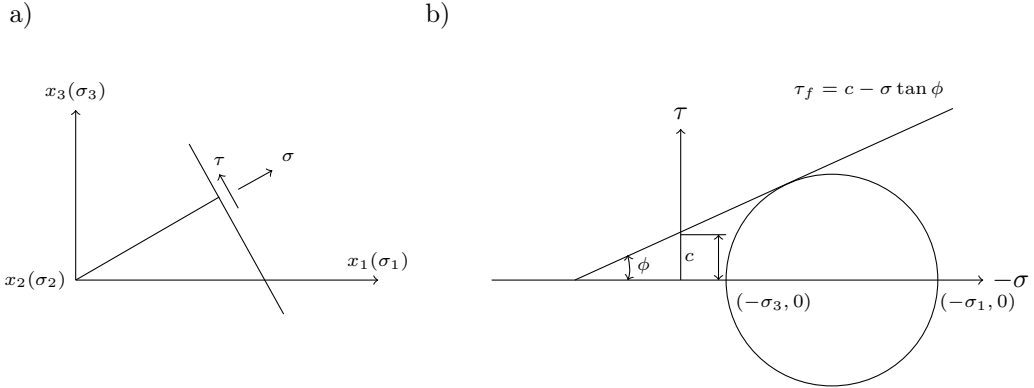


Figure 5.1: a) *The failure plane* , b) *The Coulomb criterion and Mohr's circle*.

The Mohr-Coulomb failure criterion will be discussed more thorough later in this chapter, here it is only presented to illustrate some parameters that are used to describe the shearing resistance of a soil. However, as mentioned earlier the strength of soil in reality may depend on a large number of parameters, i.e.

$$\tau_f = F(e, c, \sigma, \phi, C, H, T, \varepsilon, \dot{\varepsilon})$$

where  $e$  is the void ratio,  $C$  the soil composition,  $H$  represents the stress history and  $T$  the temperature. The parameter  $\varepsilon$  denotes, as in the previous, the strain state and  $\dot{\varepsilon}$  the strain rate. Depending on the material model used to model the soil behavior any number of these parameters needs to be established, this is generally done using specified soil tests. It is somewhat questionable to how precise the soil parameters need to be determined when soil behavior is predicted as earth materials often are in-homogenous and varying both in composition and strength. When simulations of soil behavior are done the effect of these material variations will often be neglected as the amount of soil tests that would be needed to catch the material variations is often too expensive and time consuming to conduct. It is instead the general material properties that are of interest for most simulations.

To be able to understand and evaluate the credibility of the results from a computational simulation it is also important to have knowledge of different failure

and deformation behaviors for different soils. Some typical stress-strain relations for soils are illustrated in Figure 5.2,

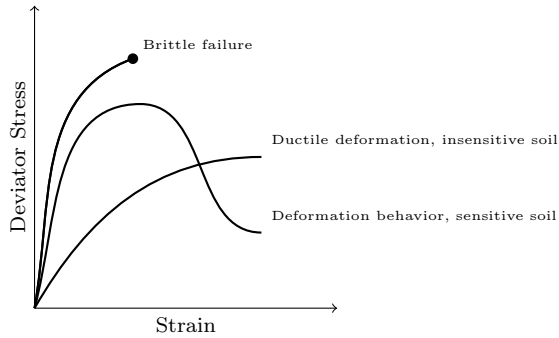


Figure 5.2: a) Typical stress-strain behavior for different soils (Mitchell and Soga; 2005).

From Figure 5.2 it can be seen that the stress-strain behavior ranges from very brittle to ductile behavior (Mitchell and Soga; 2005). Table 5.1 indicates which soils that show ductile and brittle behavior, which may be useful to evaluate the results from computational calculations.

Table 5.1: Describing different soils failure behavior.

quick clays cemented soils heavily overconsolidated clays dense sands	(Brittle failure)
insensitive clays remolded clays loose sands	(Ductile deformation)

There are indeed many other factors that affect how a soil behaves during loading, i.e. load history, effective confining pressure and consolidation rate. Where the term *consolidation* describes the compaction of a soil, that is consolidation describes the soil volume change as the water content reduces due to increased overburden or change in the groundwater level and the confining pressure is the pressure of surrounding fluids (Mitchell and Soga; 2005).

It should also be mentioned that the soil stiffness generally decreases with increased shear strain, which is illustrated in Figure 5.3.

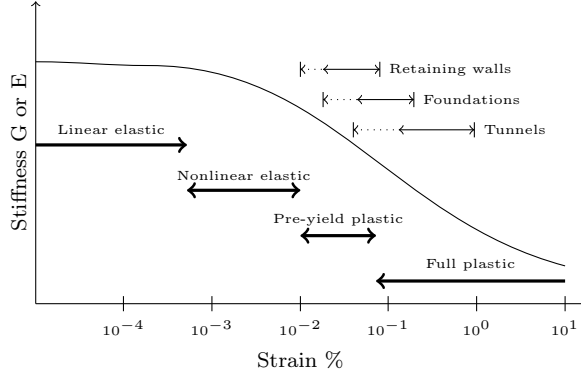


Figure 5.3: a) *Stiffness degradation curve and the strain levels observed during construction of typical geotechnical structures Mitchell and Soga (2005).*

The initial values for the stiffness parameters  $G$  and  $E$  depend on the confining pressure and the packing conditions of the soil particles and are often determined from empirical equations

$$E_{max} = A_E F_E(e) \sigma'_{ij}{}^{m_E} \quad (5.5)$$

$$G_{max} = A_G F_G(e) p'{}^{m_G} \quad (5.6)$$

Where  $F_E(e)$  and  $F_G(e)$  are functions of the void ratio,  $p'$  the effective confining pressure and  $\sigma'_{ij}$  the effective stress in respective direction, (Mitchell and Soga; 2005).

As the most basic concepts of soil behavior have been introduced the following sections will discuss the most common material models used for computational calculations of soil behavior.

## 5.2 Mohr-Coloumb

The Mohr-Coulomb failure criterion is the most popular failure criterion in soil mechanics and was first presented in 1773 by Charles-Augustin de Coulomb, and was the first criterion to account for the hydrostatic stress. According to

the Mohr-Coulomb criterion the shear strength increases with increasing normal stress,

$$|\tau_f| = c - \sigma' \tan \phi \quad (5.7)$$

where  $\tau$  is the shear stress on the failure plane,  $c$  the material cohesion,  $\sigma'$  the normal effective stress on the failure surface and  $\phi$  the angle of internal friction. In Figure 5.4 the Mohr-Coulomb criterion is illustrated with help of the Mohr circle.

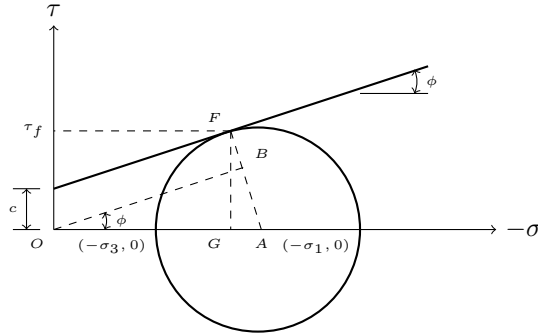


Figure 5.4: *The Mohr-Coulomb criterion and Mohr's circle.*

With Figure 5.4 as reference the Mohr-Coulomb criterion will be derived in the following.

$$-\frac{\sigma_1 - \sigma_3}{2} = AB + BF \quad (5.8)$$

That can be rewritten as,

$$-\frac{\sigma_1 - \sigma_3}{2} = OA \sin \phi + c \cos \phi \quad (5.9)$$

Inserting that  $OA = -\frac{1}{2}(\sigma_1 + \sigma_3)$  into (5.9) one obtains,

$$-\frac{\sigma_1 - \sigma_3}{2} = -\frac{\sigma_1 + \sigma_3}{2} \sin \phi + c \cos \phi \quad (5.10)$$

Where  $\sigma_1$  and  $\sigma_3$  are the major and minor principal stresses respectively. It also clear from (5.10) that the Mohr-Coulomb criterion is independent of the effects of the intermediate principal stress (Desai and Siriwardane; 1984). The expression in (5.10) can be projected on the deviator- or  $\pi$ -plane where it takes the form of an irregular hexagon illustrated in Figure 5.5.

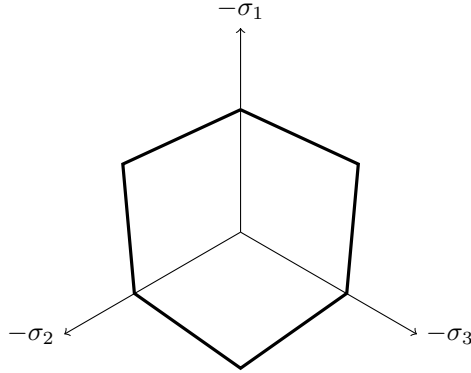


Figure 5.5: *The Mohr-Coulomb criterion on the deviator plane.*

The Mohr-Coulomb criterion states that the yield strength in compression is higher than the yield strength in tension. The Mohr-Coulomb criterion is expressed in terms of  $\sigma_1$  and  $\sigma_3$ , and as mentioned not including  $\sigma_2$ . Therefore it is inconvenient to express the Mohr-Coulomb criterion with the components of the stress tensor and consequently it becomes difficult to describe the criterion with the stress invariants  $(I_1, I_2, I_3)$ . The Mohr-Coulomb yield criterion is instead commonly described with  $(I_1, J_2, \theta)$ , defined in Chapter 3 as,

$$I_1 = \sigma_1 + \sigma_2 + \sigma_3$$

$$J_2 = \frac{1}{2}(s_1^2 + s_2^2 + s_3^2) \quad (5.11)$$

$$\theta = -\frac{1}{3} \sin^{-1} \left( -\frac{3\sqrt{3}}{2} \frac{J_3}{J_2^{3/2}} \right)$$

where  $-\pi/6 \geq \theta \geq \pi/6$  and  $J_3 = \frac{1}{3}(s_1^3 + s_2^3 + s_3^3)$ . This leads to the convectional form of Mohr-Coulomb criterion in a three-dimensional stress space as, (Desai and Siriwardane; 1984)

$$f(I_1, J_2, \theta) = I_1 \sin \phi + \sqrt{J_2} \cos \theta - \frac{\sqrt{J_2}}{3} \sin \phi \sin \theta - c \cos \phi = 0 \quad (5.12)$$

One setback to the Mohr-Coulomb criterion is that the shape of the yield surface leads to numerical difficulties when treating the plastic flow at corners of the yield surface. Another issue with the Mohr-Coulomb criterion is the conic shape

of the yield surface opening in the direction of the hydrostatic axis, see Figure 5.6.

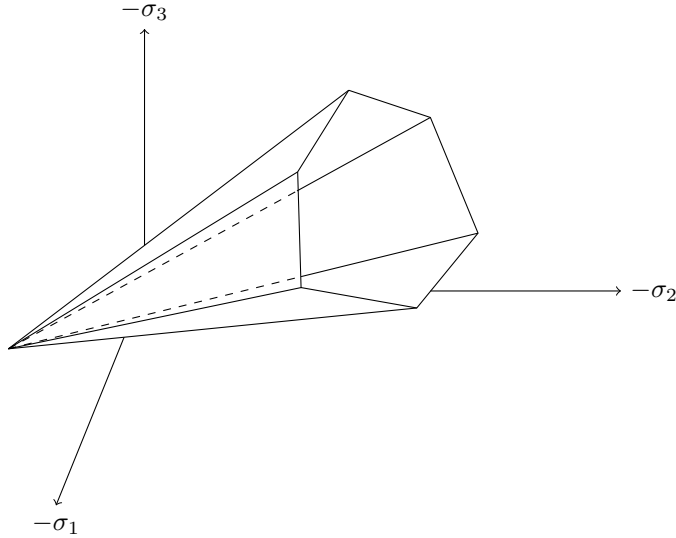


Figure 5.6: *Projection of the Mohr-Coulomb criterion in the principal stress space.*

This leads to that the Mohr-Coulomb criterion will not describe soil behavior accurately above a certain limit pressure along the hydrostatic axis. The opening in the direction of the hydrostatic axis implies that the material can bear infinite pure hydrostatic compressions without forming any plastic deformations, (Ottosen and Ristinmaa; 2005)

### 5.3 Drucker-Prager

The Drucker-Prager criterion was suggested by Drucker and Prager in 1952. The Drucker-Prager criterion can be seen a generalization to account for the effects of all principal stresses. This generalization is formed with the invariants of the stress tensor,  $I_1, J_2$  and when geotechnical stresses are considered the criterion can be written as.

$$f(I_1, J_2) = \sqrt{J_2} + \alpha I_1 - k = 0 \quad (5.13)$$

The parameters  $\alpha$  and  $k$  are positive material parameters that can be determined from the slope and interception of the yield surface plotted in the  $I_1 - \sqrt{J_2}$  plane, illustrated in figure 5.7.

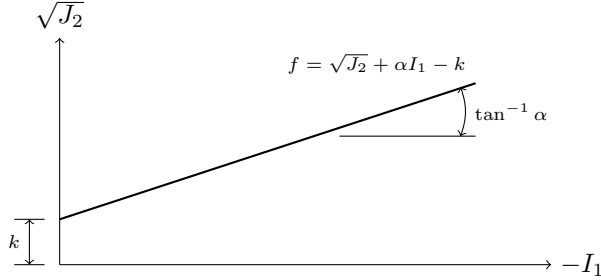


Figure 5.7: *The Drucker-Prager criterion in the meridian plane.*

The values of  $k$  and  $\alpha$  can also be expressed in terms of cohesion,  $c$ , and internal friction,  $\phi$ . However, it is important to mention that the values of  $c$ , and  $\phi$ , determined using conventional triaxial tests are different from those determined under plane strain (Desai and Siriwardane; 1984). For the conventional triaxial tests, i.e. the three dimensional case, the parameters  $k$  and  $\alpha$  can be determined either by matching to the compressive meridian of the Mohr-Coulomb criterion by

$$\alpha = \frac{2}{\sqrt{3}} \frac{\sin \phi}{(3 - \sin \phi)} \quad (5.14)$$

$$k = \frac{6}{\sqrt{3}} \frac{c \cos \phi}{(3 - \sin \phi)} \quad (5.15)$$

or matched to the tensile meridian of the Mohr-Coulomb criterion using

$$\alpha = \frac{2}{\sqrt{3}} \frac{\sin \phi}{(3 + \sin \phi)} \quad (5.16)$$

$$k = \frac{6}{\sqrt{3}} \frac{c \cos \phi}{(3 + \sin \phi)} \quad (5.17)$$

The matching of meridian indicates if the Drucker-Prager criterion is matched to either the compressive or the tensile meridian of the Mohr-Coulomb criterion, this is illustrated in Figure 5.8.

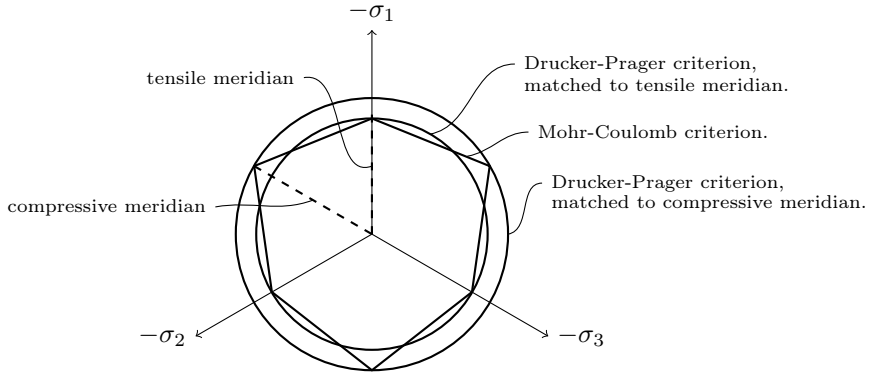


Figure 5.8: *Projection of the Drucker-Prager criterion matched to the Mohr-Coulomb criterion on the deviator plane.*

For the case of plane strain, common to use when two dimensional calculations are done for soil, the material parameters  $k$  and  $\alpha$  are instead determined according to

$$\alpha = \frac{\tan \phi}{(9 + 12 \tan^2 \phi)^{1/2}} \tag{5.18}$$

$$k = \frac{3 c}{(9 + 12 \tan^2 \phi)^{1/2}}$$

From Figure 5.8 it can be seen that the Drucker-Prager criterion takes the form of a circle when viewed in the deviator plane. This property of the Drucker-Prager criterion makes it more stable in numerical calculations than the Mohr-Coulomb criterion and therefore often used in commercial softwares for modeling the behavior of friction materials. It is however important to mention that the matching to the Mohr-Coulomb criterion displayed in Figure 5.8 can be done with other methods than those illustrated in this section.

One set back that the Drucker-Prager criterion has in common with the Mohr-Coulomb criterion is the conic shape of the yield surface that opens in the direction of the hydrostatic axis, see Figure 5.9.

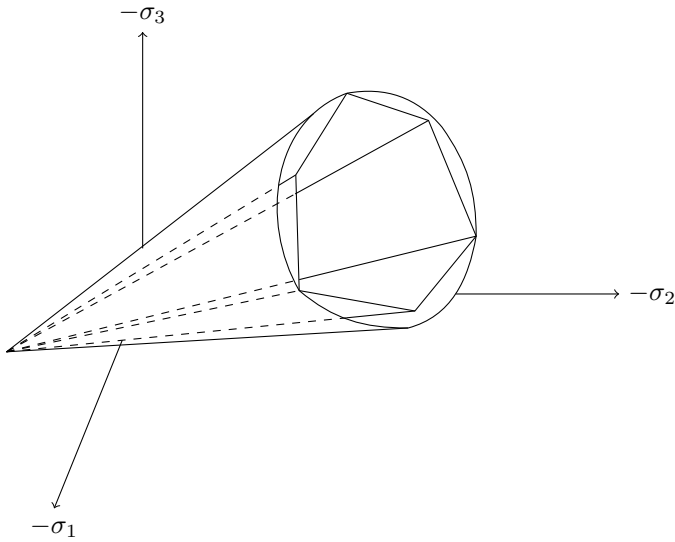


Figure 5.9: *The Drucker-Prager criterion matched to the compressive meridian of the Mohr-Coulomb criterion in the principal stress space.*

## 5.4 Elliptic cap

One way to overcome the problem with connecting the volumetric strain and the hydrostatic stress is to add a so-called cap on the yield criterion. This cap often takes the form of an ellipse and closes the stress space so that purely hydrostatic compression will give rise to plasticity, this is illustrated in Figure 5.10.

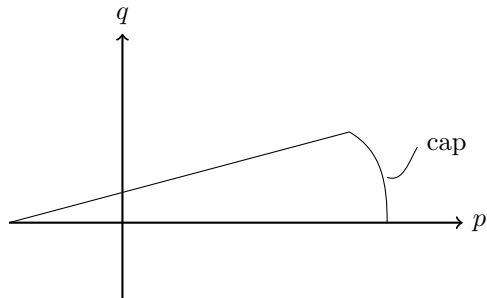


Figure 5.10: *Yield surface supplemented by a cap displayed in the plane of the invariants  $p$ ,  $q$ .*

Although the cap method has proven to achieve improved results for some material models such as Mohr-Coulomb and Drucker-Prager, it turns out that this method of improving associated plasticity does not model the important plastic volume changes in a satisfying manner. This is due to that with associated plasticity the plastic volume changes are controlled by the shape of the yield surface, which has shown to be a far too restricted format. Therefore non-associated plasticity is recommended when modeling the behavior of friction materials, (Ottosen and Ristinmaa; 2005).

# 6 Software introduction

In this chapter a brief introduction to the three computer softwares used in this report will be done, starting off by giving a general presentation of each program, presenting the material models implemented in all three softwares. As simulations done during the work with this report have shown that results from the three softwares diverge somewhat from each other a discussion will be held on some differences in how two of the most common material models used in geotechnical calculations have been implemented in the softwares, namely *Mohr-Coulomb* and *Drucker-Prager* presented in Chapter 5.

This will be followed by a parameter study done to establish how the numerical results may differ for these common material models. The study is done by simulating a triaxial compression test, where a simple axisymmetric geometry is used.

## 6.1 Introduction of Plaxis 2D

Plaxis 2D is a finite element program purposely built to calculate deformations and perform stability analysis for two-dimensional geotechnical applications. In Plaxis 2D the user has two options in how to idealize the real problem at hand, either with plane strain conditions or as an axisymmetric problem. The user interface in Plaxis 2D consists of three sub programs, Input, Calculations and Output. As the software is purposely created to handle geotechnical engineering problems there exists generalized methods in how to set up common geotechnical problems such as excavations handled in this report (Brinkgreve; 2011).

## 6.2 Introduction of Z-Soil

Z-Soil is a finite element program developed to model geotechnical constructions, foundations and underground flow. Z-soil supports axisymmetric and plane strain conditions as well as three-dimensional analysis, all types of analysis supports calculation with single or 2-phase materials. As mentioned for Plaxis above, Z-soil also has generalized methods in how to establish common geotechnical problems (Zace Services Ltd; 2003).

## 6.3 Introduction of COMSOL Multiphysics

Comsol Multiphysics is a general finite element software, it is hence possible to model a number of physical phenomena ranging from microscale electro-mechanical systems to chemical reactions. This is done in different physical modules, these modules can also be used together to create multiphysics analysis. In this report three of these physical modules have been used, the Structural Mechanics Module, the Geomechanics Module and the Subsurface Flow module. Where the Geomechanics Module is an extension of the Structural Mechanics Module that handles the nonlinear material models used to model soil behavior. During the work with this report version 4.2 of Comsol Multiphysics have been used (Comsol; 2011).

## 6.4 Sign convention

It is worth mentioning the sign convention in the three softwares as it is not obvious. Engineering analysis of soil and rock behavior for most cases are concerned with compressive stresses. Therefore, it is common in geotechnical applications to use opposite sign convention, that is, in geotechnical applications it is common to use positive sign for compressive stresses as they are more common than tensile stresses. However, all three softwares used during this work use the sign convention from continuum mechanics during the calculations, that is negative sign for the compressive stresses. There is however a difference in how the sign convention is used for the principal stresses in Plaxis 2D compared to Z-soil and Comsol Multiphysics. In Plaxis 2D the effective principal stresses are arranged accordingly

$$\sigma'_1 \leq \sigma'_2 \leq \sigma'_3 \tag{6.1}$$

In Z-soil and Comsol Multiphysics on the other hand the principal stresses are arranged as

$$\sigma_1 \geq \sigma_2 \geq \sigma_3 \quad (6.2)$$

The difference in sign convention does not affect the calculations but it is important to have in mind how the principal stresses are defined when the results from a calculation is evaluated.

## 6.5 Soil material models

As the problem at hand has been idealized and the geometry established a suitable material model for the soil has to be chosen. Which material model to use depends on a number of factors, i.e. the type of soil, available material parameters, the type of study performed and many more. Therefore one important factor when evaluating simulation tools is to compare the material models the softwares handle, as the material models in some extent determine which problems that are possible to simulate with each software. Table 6.4 lists all the material models that can be used to model soil behavior in the three computer softwares.

Table 6.1: *The material models that can be used to model soil and rock behavior in the three computer softwares.*

Material models for soil	Plaxis	Z-soil	Comsol
Linear elastic model	x	x	x
Mohr-Coulomb model	x	x	x
Drucker-Prager model		x	x
Cam-Clay / Soft soil model	x	x	x
Hardening soil model	x	x	
Hardening soil small strain model	x	x	
Soft soil creep model	x		
Matsuoka-Nakai model			x
Lade-Duncan model			x

Even though some material models have the same name and exists in all three softwares it is not certain that these material models will give exactly same results when used in the three softwares. These differences might depend on a number of factors, such as element types, solvers and due to how the material models

have been implemented. As thorough review of this matter would be too extensive for this report, only a brief summary of some of the differences regarding how the Mohr-Coulomb criterion has been implemented in the softwares will be discussed.

### 6.5.1 Linear elastic model

A linear elastic model exists in all three computer softwares and is generally not suited to model soil behavior. The linear elastic model is formed from *Hook's generalized law* described in Chapter 4. The linear elastic model can instead be used to model massive structures interacting with soil layers, the model shows unlimited strength, which must be taken into account using the model.

Table 6.2: *Required parameters using the linear elastic model.*

Parameters	Plaxis	Z-soil	Cmsol
Young's modulus, $E$	x	x	x
Poisson's ratio, $\nu$	x	x	x

### 6.5.2 Mohr-Coloumb model

Mohr-Coulomb failure criterion is the most widely used material model in soil mechanics. It was first developed by Charles-Augustin de Coulomb and it was the first material model to take the hydrostatic pressure into account. The Mohr-Coloumb criterion states that yielding occurs when,

$$|\tau_f| = c - \sigma \tan \phi \quad (6.3)$$

where  $\tau$  is the shear stress on the failure plane,  $c$  the material cohesion,  $\sigma$  the normal effective stress on the failure surface and  $\phi$  the angle of internal friction. The Mohr-Coulomb criterion is an elastic perfect plastic material model and it may in some cases overestimate the soils hydrostatic compressive strength. Using the Mohr-Coulomb model it is important to consider that in the general case the criterion does not consider the hardening or softening behavior and may therefore not give a credible result for all calculations.

Table 6.3: *Required parameters using the Mohr-Coulomb model.*

Parameters	Plaxis	Z-soil	Comsol
Young's modulus, $E$	x	x	x
Poisson's ratio, $\nu$	x	x	x
Angle of internal friction, $\phi$	x	x	x
Cohesion, $c$	x	x	x
Dilation, $\psi$	x	x	

### Implementation of Mohr-Coulomb criterion

As there are differences in how material models are implemented in any computer software, this section will briefly discuss some of these differences regarding the Mohr-Coulomb model. This section does not aim to give a full review of how the Mohr-Coulomb criterion has been implemented in the three softwares but rather point out some differences that have become obvious during the work with this report.

All three softwares use the theory of non-associated plasticity presented in Chapter 4, equation (4.44), where one yield function and one plastic potential function is used to determine the plastic strains. The yield functions used in the three softwares are all based on equation (5.10) or (5.12) with some variations. For example in Plaxis the Mohr-Coulomb yield criterion is formulated using the principal stresses using six yield functions to represent the hexagonal cone in the principal stress space, see Figure 5.6. The equations in (6.4) show these six yield functions used in Plaxis (Brinkgreve; 2011).

$$\begin{aligned}
 f_{1a} &= \frac{1}{2}(\sigma'_2 - \sigma'_3) + \frac{1}{2}(\sigma'_2 + \sigma'_3) \sin \phi - c \cos \phi \leq 0 \\
 f_{1b} &= \frac{1}{2}(\sigma'_3 - \sigma'_2) + \frac{1}{2}(\sigma'_3 + \sigma'_2) \sin \phi - c \cos \phi \leq 0 \\
 f_{2a} &= \frac{1}{2}(\sigma'_3 - \sigma'_1) + \frac{1}{2}(\sigma'_3 + \sigma'_1) \sin \phi - c \cos \phi \leq 0 \\
 f_{2b} &= \frac{1}{2}(\sigma'_1 - \sigma'_3) + \frac{1}{2}(\sigma'_1 + \sigma'_3) \sin \phi - c \cos \phi \leq 0 \\
 f_{3a} &= \frac{1}{2}(\sigma'_1 - \sigma'_2) + \frac{1}{2}(\sigma'_1 + \sigma'_2) \sin \phi - c \cos \phi \leq 0 \\
 f_{3b} &= \frac{1}{2}(\sigma'_2 - \sigma'_1) + \frac{1}{2}(\sigma'_2 + \sigma'_1) \sin \phi - c \cos \phi \leq 0
 \end{aligned} \tag{6.4}$$

In Z-soil two versions of the Mohr-Coulomb criterion exist, one using the hexagonal cone shape presented earlier and one modified version of the criterion where the yield surface is approximated by a smooth single-surface function. However, in this report only the basic version of the Mohr-Coulomb criterion has been used. For this classical Mohr-Coulomb criterion Z-soil uses a similar method as Plaxis to implement the yield surface, with the difference that only four yield functions are used (Zace Services Ltd; 2003). The four yield functions are presented in (6.5).

$$f_1 = \sigma_1 - \sigma_3 \frac{1 - \sin \phi}{1 + \sin \phi} - \frac{2c \cos \phi}{1 + \sin \phi} = 0 \quad (6.5)$$

$$f_2 = \sigma_1 - \sigma_2 = 0 \quad (6.6)$$

$$f_3 = \sigma_2 - \sigma_3 = 0 \quad (6.7)$$

$$f_4 = \sigma_1 - \sigma_t = 0 \quad (6.8)$$

Where  $f_4$  is optional, and controls the tension cut off. In Comsol Multiphysics the yield function used in the Mohr-Coulomb model is defined with the stress invariants presented in Chapter 2. The yield function used is given by

$$f = \sqrt{J_2}m(\theta) + \alpha I_1 - k \quad (6.9)$$

according to (Comsol; 2011). Where the parameters  $\alpha = \sin(\phi)/3$  and  $k = c \cos \phi$ . The parameter  $m(\theta)$  is given from,

$$m(\theta) = \cos\left(\theta - \frac{\pi}{6}\right) - \sqrt{\frac{1}{3}} \sin \phi \sin\left(\theta - \frac{\pi}{6}\right)$$

One other issue regarding the yield surface for the Mohr-Coulomb criterion is the fact that the criterion allows for tensile stresses in the material when cohesion is introduced. Most soils however do not carry any or only very small tensile stresses. This issue is handled in Plaxis and Z-soil by letting the user determine a value to "cut-off" the tension stresses. No predefined method of doing this in Comsol has been found, although it would be possible for the user to define such a restriction to the criterion manually. This would however be more time consuming and demand more from the user than the methods in Z-soil and Plaxis.

The next issue to address is the plastic potential functions. In Z-soil and Plaxis these are defined similar to the yield functions with the difference that they in both cases are dependent on the angle of dilation and not the angle of internal friction. Where the angle of dilation,  $\psi$ , governs the dilatation, that is the volume increase, in the material during yielding.

In Comsol however no way of controlling the material dilatation has been found and the plastic potential function is instead user-defined smoothed version of the yield function. For the Mohr-Coulomb criterion the user can choose between a function matched to either the tensile or compressive meridian of the Drucker-Prager criterion (Comsol; 2011).

There are of course other differences in the softwares that might have a larger impact on the results, but this discussion has illustrated that even though the three softwares have implemented the same basic theory for a rather simple material model there are differences. In Section 6.6 the impact of these differences are explored further with a numerical simulation of a triaxial test.

### 6.5.3 Drucker-Prager model

The Drucker-Prager criterion is often seen as the numerically most suitable criterion to model the behavior of frictional materials and was formed in 1952 by Drucker and Prager. According to the Drucker-Prager criterion yielding occurs as,

$$f(I_1, J_2) = \sqrt{J_2} - \alpha I_1 - k = 0 \quad (6.10)$$

where  $\alpha$  and  $k$  are positive material parameters which can be described using the material cohesion,  $c$ , and the angle of internal friction,  $\phi$ , see further (5.14)-(5.17), Chapter 5. The Drucker-Prager criterion has the same issues with overestimated hydrostatic compressive strength as earlier described for the Mohr-Coulomb criterion. As the yield surface is formed by a continuous function in the Drucker-Prager criterion it is more stable than the Mohr-Coloumb criterion performing numerical calculations.

Table 6.4: *Required parameters using the Drucker-Prager model.*

Parameters	Plaxis	Z-soil	Comsol
Young's modulus, $E$		x	x
Poisson's ratio, $\nu$		x	x
$\alpha$		x	x
$k$		x	x
Dilatation, $\psi$		x	

## 6.6 Simulation of Triaxial test

To investigate if there are any major differences in the numerical results between Plaxis, Z-soil and Comsol Multiphysics a simulation of a triaxial test has been performed. As the three softwares has different methods of simulating the influence of initial void ratio, water pressure and contact surfaces, which all influence the results from a calculation, the simulation is done with very simple boundary conditions. The initial void ratio will be kept at the preset levels in each software and no water pressure will be added. The simulations are done with an axial symmetric geometry with the boundary conditions according to Figure 6.1.

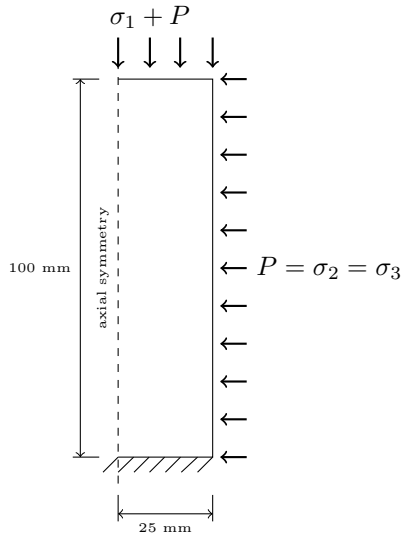


Figure 6.1: *Geometry used for simulation of triaxial compression test.*

The calculations are done in two steps, in step one the confining pressure, represented by  $\sigma_2$  and  $\sigma_3$  in Figure 6.1, is raised to 10 kPa. In step two the vertical pressure,  $\sigma_1$ , is then raised until convergence problems arise. The simulations were done as a parametric study, using six different material settings described below. As it might be interesting to compare the differences between the material models as well as the difference between the three softwares, the same material properties have been used as far as possible. During the calculations the Young's

modulus,  $E$ , the Poisson's ratio,  $\nu$  and the density,  $\rho$  are held constant,

$$E = 20[\text{MPa}]$$

$$\nu = 0.3$$

$$\rho = 1800[\text{kg/m}^3]$$

The material properties for cohesion,  $c$ , and internal friction,  $\phi$ , are varying according to Table 6.5 below.

Table 6.5: *Material setting for triaxial soil simulations.*

Case	Test#1	Test#2	Test#3	Test#4	Test#5	Test#6	unit
$c$	$2 \cdot 10^3$	$5 \cdot 10^3$	$10 \cdot 10^3$	$15 \cdot 10^3$	$2 \cdot 10^3$	$2 \cdot 10^3$	[Pa]
$\phi$	32	32	32	32	28	37	[deg]

### 6.6.1 Results for Mohr-Coloumb criterion

From 6.2 below it can be seen that initial yielding takes place at a similar magnitude of the applied force,  $\sigma_1$ , for the Mohr-Coulomb criterion. This is

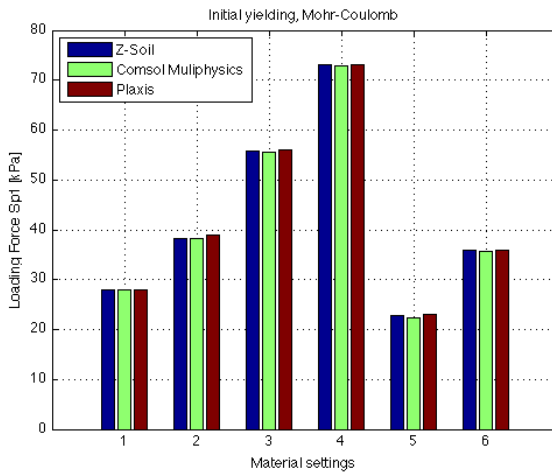


Figure 6.2: *Figure displaying force level,  $\sigma_1$ , at initial yielding with the Mohr-Coulomb criterion as material model.*

## 6.6. SIMULATION OF TRIAXIAL TEST

It is also of interest to observe the stress distribution for the three softwares as a control of how the geometry model behaves in the three softwares. In Figure 6.3 the distribution of the maximum normal stress is displayed at applied vertical pressure,  $\sigma_1 = 28$  kPa. The results from the simulations of the compressive triaxial test shows that for the Mohr-Coulomb criterion at totally drained conditions the three softwares provide similar results for both stress distribution and initial yielding. Convergence problems also arise at similar confining pressures.

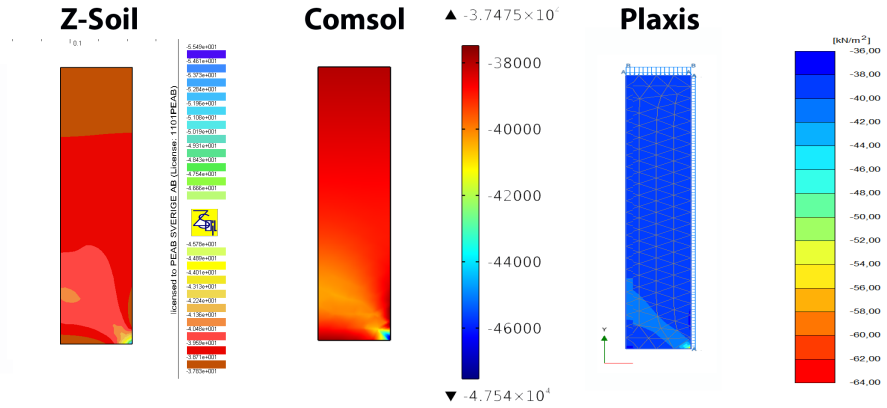


Figure 6.3: Stress distribution for the maximum normal stress, denoted  $\sigma_1$  in Plaxis and  $\sigma_3$  in Z-Soil and Comsol Multiphysics, at vertical pressure = 28kPa. The results are given for material parameters from test #1 in Table 6.5.

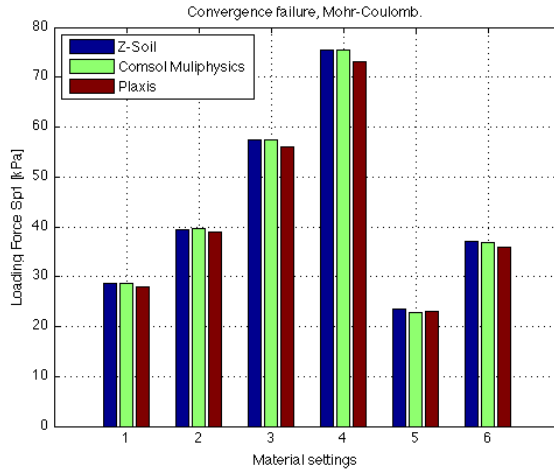


Figure 6.4: Force level,  $\sigma_1$ , at convergence failure with the Mohr-Coulomb criterion as material model.

### 6.6.2 Results for Drucker-Prager criterion

The same procedure has been used to perform the same calculations using the Drucker-Prager criterion in Z-soil and Comsol Multiphysics. As Plaxis 2D does not have the Drucker-Prager criterion implemented, the results from the Mohr-Coulomb criterion from Plaxis 2D are displayed along with the results using the Drucker-Prager criterion in Z-soil and Comsol Multiphysics.

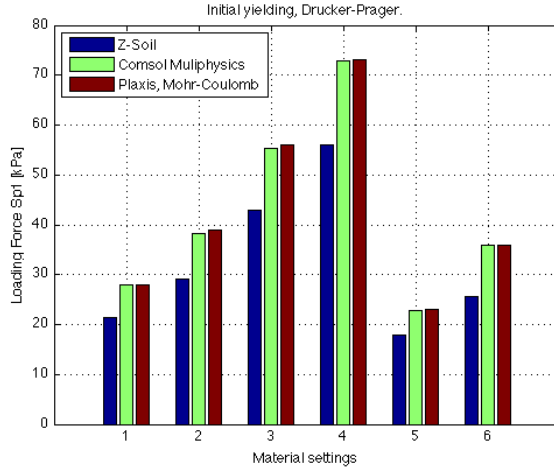


Figure 6.5: Figure displaying force level,  $\sigma_1$ , at initial yielding with the Drucker-Prager criterion as material model.

It can be seen in the Figure 6.5 that the initial yielding occurs at lower confining pressure using the Drucker-Prager criterion in Z-soil. In Comsol the initial yielding using the Drucker-Prager criterion occurs at approximately the same confining pressure as when the Mohr-Coulomb criterion is used. It is also interesting to see that there is a rather large difference between the results from Z-soil and Comsol using the Drucker-Prager criterion, which was not the case for the Mohr-Coulomb criterion. Reasons for this might be that in Comsol Multiphysics the user has an option to make the Drucker-Prager criterion match either the tensile or compression meridian also for two dimensional calculations, whereas Z-soil uses equation (5.18). Additional tests were performed in Comsol Multiphysics with the Drucker-Prager criterion matched to the tensile meridian of the Mohr-Coulomb criterion. The results showed that the force level when initial yielding occurs was lower then the results from Z-soil presented in Figures 6.5 and 6.6.

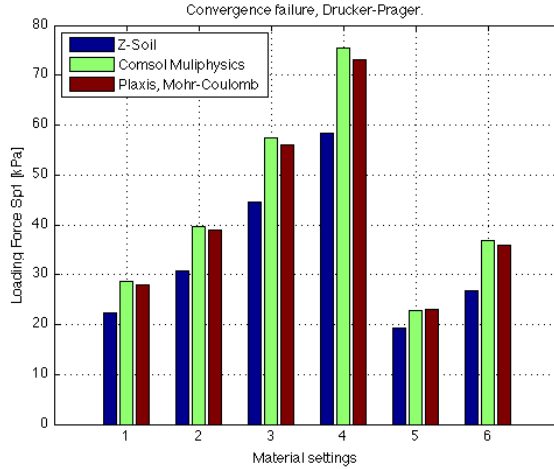


Figure 6.6: Force level,  $\sigma_1$ , at convergence failure with the Drucker-Prager criterion as material model.

From the results it could be seen that the spreading of the yielding throughout the elements was smoother and that more elements experienced plastic deformations using the Drucker-Prager criterion compared to when the Mohr-Coulomb criterion was used. This implies that the Drucker-Prager criterion shows more stable numerical results than the Mohr-Coulomb criterion for this simple compression test.

The effects of the matching to Mohr-Coulomb criterion in Comsol Multiphysics is illustrated in Figure 6.7. The figure also shows the convergence problem with Mohr-Coulomb criterion. This can be seen in that the red curve stops abruptly at a loading level around 40 kPa without capturing the displacements that can be seen from the calculations using the Drucker-Prager criterion.

## 6.6. SIMULATION OF TRIAXIAL TEST

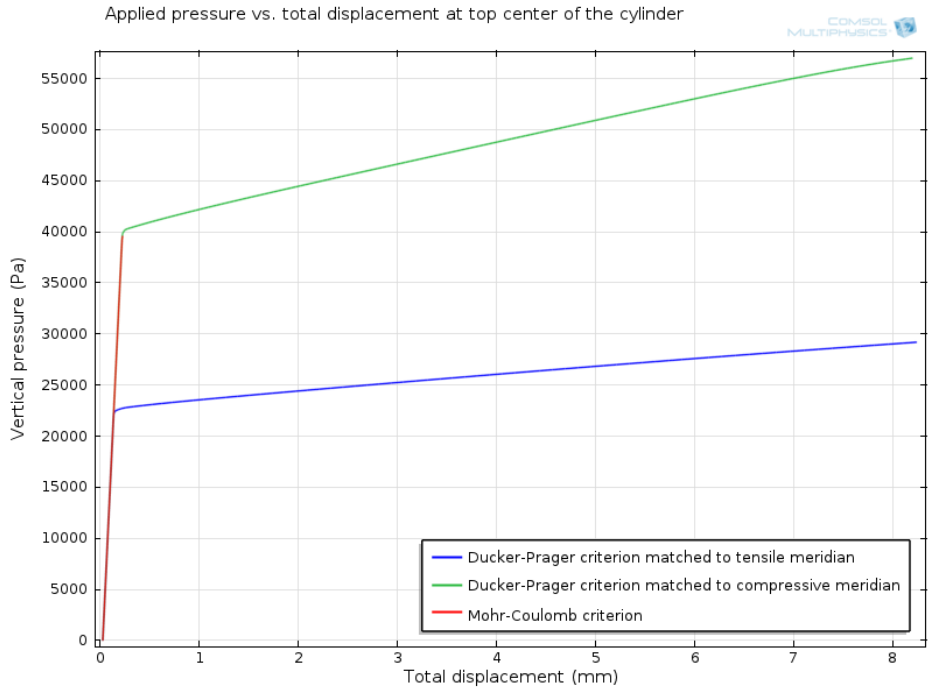


Figure 6.7: The total deformation plotted against the applied force  $\sigma_1$  at the top center of the test cylinder in Comsol.

The results from this parameter study shows the importance of choosing the appropriate matching to the Mohr-Coulomb criterion when using the Drucker-Prager criterion, as the matching affects the results greatly.

## 7 Excavation with a tie back retaining wall

In this chapter the results and methods used to simulate a simple excavation problem in the three softwares will be presented. As no real case study has been done during the work with this report the calculations performed are done according to a previous study by (Jönsson; 2007). It should be observed that this chapter does not aim to work as a tutorial, it instead merely meant to give an overview of how a simple problem can be solved using Plaxis 2D, Z-soil and Comsol Multiphysics.

The study at hand consists of a 6 meter deep and 20 meters wide excavation with a pre-stressed tie back retaining wall. The excavation is performed in two stages, with a lowering of the groundwater level inside the retaining walls before the last excavation stage takes place. Figure 7.1 shows the finished excavation that will be simulated in this chapter.

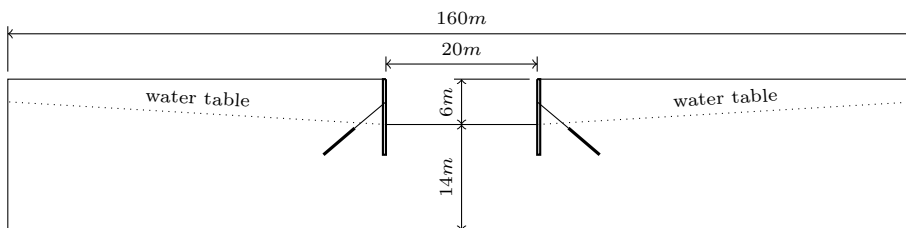


Figure 7.1: *Schematic illustration of the excavation problem.*

## 7.1 Material Parameters

The material data used in the simulations are presented in the following where Tables 7.1-7.3 list the material parameters used for the soil, retaining wall and anchoring respectively.

### Material data, soil

In the calculations the Mohr-Coulomb material model will be used to simulate the soil behavior, with soil parameters according to Table 7.1. Note that all of the parameters given in Table 7.1 are not used in all three softwares.

Table 7.1: *Material parameters for the soil.*

Material Parameter	value	[unit]	Plaxis	Z-soil	Comsol
Density unsaturated soil	1800	[kg/m <sup>3</sup> ]	x	x	x
Density saturated soil	2100	[kg/m <sup>3</sup> ]	x		
Void ratio, $e_0$	0.5	-	x	x	
Young's modulus, $E$	20	[MPa]	x	x	x
Poisson's ratio, $\nu$	0.3	-	x	x	x
Cohesion, $c$	2	[kPa]	x	x	x
Angle of internal friction, $\phi$	35	[deg]	x	x	x
Angle of dilation, $\psi$	5	[deg]	x	x	
Permeability	0.5	[m/day]	x	x	
$R_{inter}$	0.5	-	x		
$K_0$	0.43	-		x	

### Material data, retaining wall

The retaining wall is constructed in concrete and is 0.4 m wide and 10 m high. The retaining wall is modeled differently in the three softwares and therefore the material parameters used for the calculations are given in diverse formats. The different material parameters used to simulate the retaining wall are presented in Table 7.2. For all three softwares the retaining wall has been modeled with a linear-elastic material model.

Table 7.2: *Material parameters for the retaining wall.*

Material Parameter	value	[unit]	Plaxis	Z-soil	Comsol
Density	2400	[kg/m <sup>3</sup> ]	x	x	x
Young's modulus, $E$	35	[GPa]		x	x
Poisson's ratio, $\nu$	0.3	-	x	x	x
Wall thickness, $d$	0.4	[m]	x	x	x
$EA$	$14 \cdot 10^6$	[kN/m/m]	x		
$EI$	$186.7 \cdot 10^3$	[kNm <sup>2</sup> /m]	x		
Cross-sectional area, $A_x$	0.4	[m <sup>2</sup> ]		x	
Cross-sectional area, $A_y$	0.4	[m <sup>2</sup> ]		x	
Moment of inertia, $I$	$5.33 \cdot 10^{-3}$	[m <sup>4</sup> ]		x	

### Material data, anchoring cable

The anchoring of the retaining wall is done by first drilling into the soil and thereafter filling the bottom of the cavity with concrete into which a steel wire is placed. The wire is then subject to a force that anchors the retaining wall to the soil. The anchoring is modeled by one steel bar/wire element that is roughly 5 meters long and fastened into a the soil in another 5 meters, see Figure 7.4. The anchor is modeled with a linear-elastic material model in all three softwares and all material parameters used are presented in Table 7.3.

Table 7.3: *Material parameters for the anchor elements.*

Material Parameter	value	[unit]	Plaxis	Z-soil	Comsol
Young's modulus, $E$	210	[GPa]		x	x
Poisson's ratio, $\nu$	0.3	-	x	x	x
$EA$	$42 \cdot 10^3$	[kN]	x		
Cross-sectional area	$2 \cdot 10^{-4}$	[m <sup>2</sup> ]		x	x
Prestressing force	375	[MPa]		x	x

## 7.2 Finite element model

To make the finite element model as realistic as possible the excavation presented above is idealized into five calculation steps illustrating the working procedure at the construction site. Even though it would have been possible to establish the calculation procedures in different manners in the different finite element

## 7.2. FINITE ELEMENT MODEL

---

softwares, the method used to solve the excavation simulation has been chosen as similar as possible in all softwares. The calculation steps used in the simulation are presented below.

1. In-situ calculation
2. Installing the retaining wall
3. Excavation step 1
4. Installing the anchor
5. Excavation step 2

It needs to be mentioned that as Comsol Multiphysics is a general finite element software there are numerous possible ways to simulate the problem at hand and therefore the method presented in this report might not be the most effective or accurate for this type of simulation. For Plaxis and Z-Soil, on the other hand, this type of simulations are well demonstrated in the available tutorials, and the excavation is therefore modeled according to the methods presented in these tutorials.

As the problem at hand is symmetric, only one half of the excavation area needs to be modeled, therefore the boundary conditions for each simulation step can be described with Figures 7.2-7.6. How these five calculation steps have been modeled in each software will be described in the following chapter.

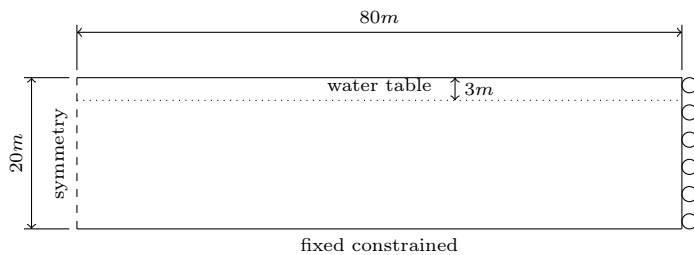


Figure 7.2: *Geometry used for simulation of excavation, calculation step 1.*

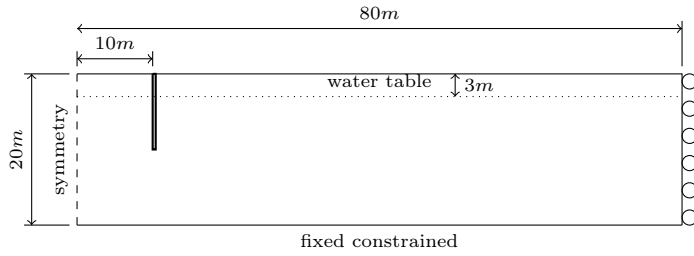


Figure 7.3: Geometry used for simulation of excavation, calculation step 2.

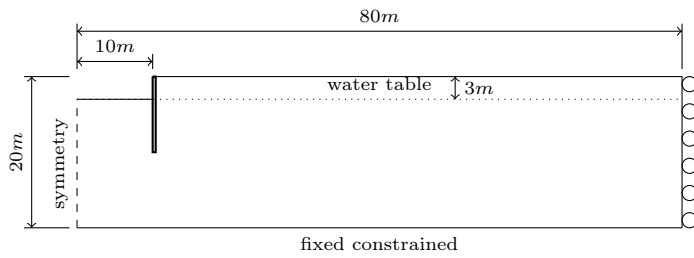


Figure 7.4: Geometry used for simulation of excavation, calculation step 3.

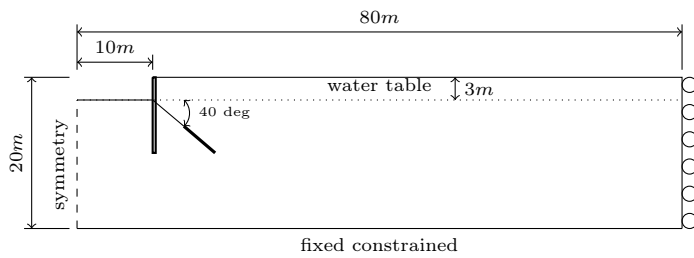


Figure 7.5: Geometry used for simulation of excavation, calculation step 4.

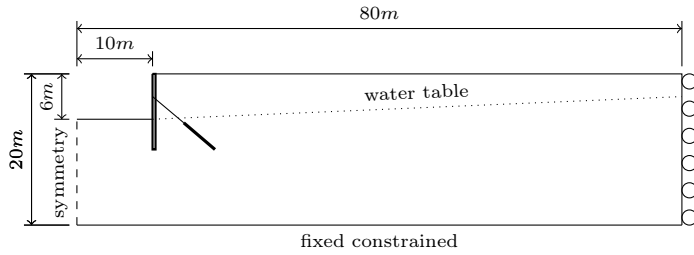


Figure 7.6: *Geometry used for simulation of excavation, calculation step 5.*

## 7.3 Plaxis

In Plaxis 2D, the problem is first defined in the Input part of the program, where the geometry, material parameters and meshing properties are first established for all elements needed during all the calculation steps. In the Calculations part of the program the elements needed for each calculation step is then activated.

### 7.3.1 Geometry model

The geometry model used in Plaxis 2D is presented in Figure 7.7 where the boundary conditions are set according to Figure 7.2 above.

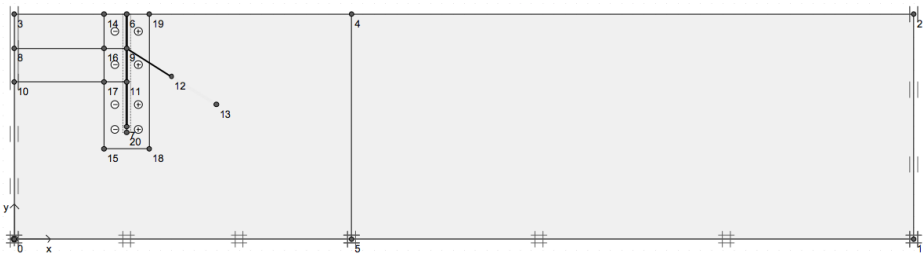


Figure 7.7: *The geometry model used in Plaxis 2D.*

In the calculations 15-node triangular elements have been used to model the soil. These elements provide a fourth order interpolation for displacement with

a numerical integration over twelve Gauss points, (Brinkgreve; 2011). The full element mesh used for the simulation is displayed in Figure 7.8.

To model the effect of the pore pressure a groundwater level is generated. In Plaxis 2D this is done by setting a *Phreatic level* at desired depth, in this case 3 meters below the surface level at the original configuration. In the last calculation step the water level is lowered inside the excavation pit by setting the phreatic level at 6 meters from the surface level.

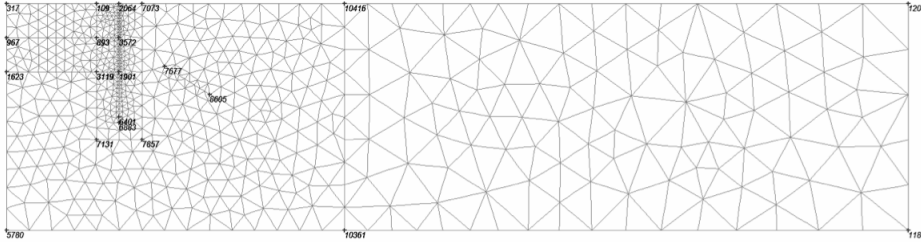


Figure 7.8: *The element mesh used in Plaxis 2D.*

## Retaining wall

The retaining wall is modeled using Plate elements in Plaxis 2D. The material properties of the plate element are given according to Table 7.2. The parameters for bending stiffness,  $EI$  and axial stiffness,  $EA$  are the most important parameters as these parameters are used to calculate the equivalent plate thickness,  $d_{eq}$ , according to (7.1) (Brinkgreve; 2011).

$$d_{eq} = \sqrt{12 \frac{EI}{EA}} \quad (7.1)$$

The plate element used in plaxis are based on Mindlin's plate theory which allows for plate deflection due to bending and shearing, (Brinkgreve; 2011). When the 15-node element is chosen to model the soil, Plaxis 2D will use a 5-node plate element with four pairs of Gaussian integration points, see Figure 7.9.

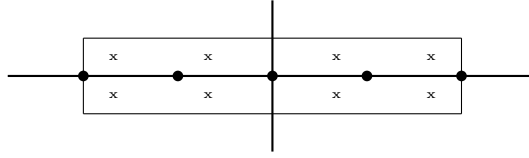


Figure 7.9: 15 node beam element used in Plaxis 2D, (Brinkgreve; 2011)

To model the interaction between the soil and the retaining wall the Interface elements in Plaxis 2D have been used. To avoid numerical problems at sharp corners in a soil-structure interaction extra caution needs to be taken for such points. If no special attention is taken to these corner points the instant change in boundary condition may lead to high stress peaks that in turn might lead to non-physical stress oscillations in the soil elements. To avoid this problem it is suggested by Brinkgreve (2011) that the interface should be extended beyond the end of the plate in the soil, see Figure 7.10 below.

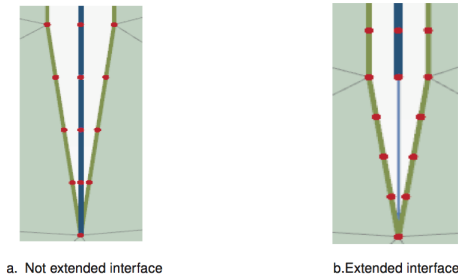


Figure 7.10: The interface with and without extension in the mesh, (Brinkgreve; 2011).

The interface elements used determine the amount of elastic deformation that will be generated by a parameter called *virtual thickness*. This virtual thickness is determined as the *virtual thickness factor* times the average element size. The virtual thickness factor is a user controlled parameter that in these calculations has been set to the default value of 0.1.

### 7.3.2 Pre-stressed ground anchor

The ground anchor has been modeled using a combination of Plaxis Geogrid element and node-to-node anchor. Where the Geogrid element is used to model

the concrete body interacting with the soil and the node-to-node anchor is used to model the anchoring rod/cable. The Geogrid element has two translational degrees of freedom in each node, in the  $x$ - and  $y$ -directions. Furthermore the Geogrid structure has no bending stiffness and can only sustain tensile forces and no compression forces, (Brinkgreve; 2011). The node-to-node anchor used to model the pre stressed bar is a spring element with constant normal stiffness. The element is used to model ties between two points, without interacting with the elements lying between these points.

The plate and anchor elements can be activated or deactivated according to the calculation steps shown in Figures 7.2-7.6. This is done using *Staged construction* as *loading input* in the calculation phase in Plaxis 2D which will be discussed in the following.

### 7.3.3 Calculation phase

After that the model has been established and all material parameters set according to Tables 7.1-7.3 the different calculation steps are defined in the calculation phase of Plaxis 2D. For this excavation problem five calculation steps have been used according to Figures 7.2-7.3. For all steps *Plastic* calculations have been used and *Staged construction* as *Loading input*, whereas all other parameters have been left at the default settings.

#### Initial phase, (phase 0)

In the initial phase the initial stress conditions in the soil are calculated using the K0 procedure. In this calculation step all the soil clusters are activated but none of the structural elements. The elements are deactivated using the Staged construction mode. The Phreatic level also needs to be turned on using the *Water condition mode*.

#### Phase 1

In calculation step 2, the retaining wall needs to be activated. This is done in the Staged construction mode by activating the plate elements and all the interface elements. Also the interface elements along the plate elements needs to be activated in the Water condition mode, this is done to set the interface elements to impermeable during the ground water calculations.

### Phase 2

In the third calculation step, the top layer of soil is removed from the calculations. This is done by de-activating the top soil cluster in the Staged construction mode.

### Phase 3

In the fourth calculation step the Geogrid and node-to-node anchor elements are activated in the Staged construction mode. In the node-to-node anchor pre-stressing force is set to 75 kN/m.

### Phase 4

In the last calculation step the final three meters of excavation is modeled by de-activating the second cluster inside the excavation using the Staged construction mode. In the Water condition mode the Phreatic level is lowered inside the excavation according to Figure 7.6.

## 7.4 Z-soil

When creating a new finite element model in Z-soil it is efficient start by defining all materials, load functions and existence functions before starting the preprocessor, which is the part of the program where the geometry is outlined and mesh generated. The materials used in the calculations are presented in Tables 7.1-7.3.

### 7.4.1 Existence functions

In Z-soil so-called existence functions are used to determine when loads, elements and boundary conditions are activated during the calculations. In Table 7.4

Table 7.4: *Existence functions used in Z-soil.*

Nr	Name	Time activated	Time de-activated
1	wall	2	6
2	soil layer 1	0	3
3	anchor	4	6
4	anchor prestress	4	5
5	soil layer 2	0	5
6	continuity	0	2
7	contact wall-soil	2	6
8	lowered water level	5	6

These existence functions are connected to the corresponding elements as the geometry is defined. It might be necessary to mention that existence function number 6, called continuity, is used to neglect the wall elements in the initial stress calculations.

### 7.4.2 Load functions

In Z-soil load functions are used to establish how fast a loading or unloading procedure should take place. The load functions can also be used to ramp an excavation step over time. In these calculations three load functions were used, one for each excavation step and one for the pre-stressing of the anchor truss. The three load functions used are presented in Table 7.5.

Table 7.5: *Load functions used in Z-soil.*

Nr	Name	Time step	Function value
1	Soil layer 1	0	1
		2	1
		3	0
2	Soil layer 2	0	1
		4	1
		5	0
3	Anchor pre-stress	1	0
		4	0
		5	1

The Load functions are just like the existence functions connected to their corresponding geometry parts when the elements are created in the preprocessor.

### 7.4.3 Geometry model

The geometry outline used in Z-soil looks much the same as the geometry outline used in Plaxis 2D, presented in Figure 7.7. In Z-soil however the user has more control over how the element mesh is generated, for each surface in the geometry the user may determine how many elements each side should be divided into as long as the neighboring surfaces have compatible meshes.

To model large surfaces in two-dimensional calculations with Z-soil, called *continuum*, there are two types of elements to chose from. One triangular element with 3-nodes and one Gauss point and one rectangular 4-node element with four Gaussian stress points which is the element type used in these calculations (Zace Services Ltd; 2003). The element mesh used during the calculations are presented in Figure 7.11.

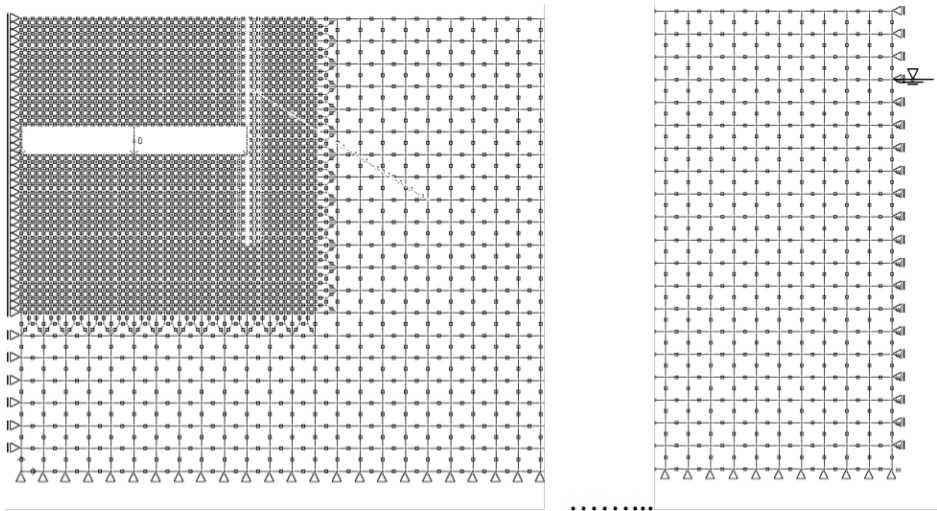


Figure 7.11: *The element mesh used in Z-soil.*

As can be seen in Figure 7.11 the element mesh is made coarser in the areas further away from the excavation. This is to save computational time. The coarse mesh consists of one by one meter elements. In the area around the retaining

wall these elements have been refined by dividing each element into nine smaller rectangular elements.

The elements inside the excavation have to be coupled to the corresponding existence and load functions described earlier. That is, all the elements from zero to three meters depth inside the excavation pit are assigned existence function 2 and load function 1, whilst the elements three to six meters depth are assigned existence function 5 and load function 2.

It is also in the preprocessor that the ground water conditions are established. This has been done by establishing a hydrostatic head 3 meters below the ground level, for the first four calculation steps. In the last calculation step the hydrostatic pressure is set to zero at the bottom of the excavation using existence function 8.

#### 7.4.4 Retaining wall

In Z-soil the retaining wall has been modeled using a beam, which is based on the Timoshenko beam theory, which is equivalent to Mindlin's plate theory used in Plaxis 2D. That is the theory takes into account shear deformation and rotational inertia effects. The beam elements have three degrees of freedom in each node, two for displacements and one rotation (Zace Services Ltd; 2003). The material parameters used for the beam element in Z-soil can be seen in Table 7.2 and the beam elements are assigned existence function 1 in Table 7.4

In Z-soil the interaction between the soil and beam elements are governed by creating interface elements along both sides of the beam element. The Interface elements can be used both to create a continuity when the beam elements are deactivated and to create a contact surface between the beam and continuum elements. When a contact surface is established an elasto-plastic friction is added to the calculations as well as permeability can be set to govern the water flow through the surface (Zace Services Ltd; 2003). In these calculations the interface elements are assigned existence functions 6 and 7, and for the contact surface the interface parameters have been set to be impermeable and with a friction angle at 17 degrees. All other parameters have been set to zero.

#### 7.4.5 Pre-stressed ground anchor

The anchor has been modeled using truss elements in Z-soil. The truss elements only carry normal forces and no moment is generated in a truss element. The truss element has no friction along the sides of the elements and is hence only

in contact with the neighboring surface in the truss element nodal points. The truss elements do not need to be attached to a specific node in the continuum element, in this case the soil, instead the displacements generated from the truss element are spread onto all nodes of the soil element at hand (Zace Services Ltd; 2003).

Thanks to the fact that the truss elements does not need to be attached to a specific node makes it possible to use the truss elements to model both the concrete injection and the anchor bar. This is done by letting the truss element that represents the pre stressed bar consist of a five meters long bar element with one node coupled to the beam element and on node coupled to a soil element. The concrete is then modeled by letting another five meters long truss element represent the injection, this truss element is then divided into 8 shorter truss elements that have both ends coupled to a soil element.

The truss elements are then assigned the existence function representing the anchor from Table 7.4.

### 7.4.6 Calculations

In Z-soil the calculation is defined under the *Analysis and Drivers definition* menu where a number of different solvers exist. For this excavation model the problem concerns deformation and groundwater flow, which in Z-soil exists as a predefined solver, called Deformation+Flow. It is also under the *Analysis and Drivers definition* that the calculation steps are defined. The calculation steps used for the problem are given in Table 7.6.

Table 7.6: *Analysis and Drivers settings used in Z-soil.*

Nr	Driver	Type	Initial time	Finish time	Increment
1	Initial state		0.5	1	0.1
2	Time Dependent	Driven Load	1	3	1
3	Time Dependent	Driven Load	4	6	0.2
4	Stability	tg(phi),c	1	3	0.1

#### 1. Initial State

In Z-soil the initial state calculations are performed and established automatically depending on which problem type the user has defined. For Deformation+Flow problems the initial state calculations first perform a steady state flow calculation

according to the pressure boundary conditions established in the preprocessor. The results from the steady state flow calculations are then used in an initial state deformation calculation, which is performed with the K0 procedure. In the initial state deformation calculations the load case then consists of the body load induced by the pressure gradient (Zace Services Ltd; 2003). As the gravity enforced body load can be rather large the calculation is performed incrementally, the size of the calculation steps is indicated in the Increment column in Table 7.6.

## 2. Time Dependent

For the driven load, time dependent solver the calculations consist of two substeps for each time increment, first a steady state flow calculation solving the pore pressure distribution. The results from the flow calculations are then used to determine the deformations in the second substep. Each calculation step starts from the results in the previous calculation step. In the first time step, from  $t=1$  to  $t=2$ , the retaining wall is activated, as established in Table 7.4. In the second time step, from  $t=2$  to  $t=3$ , the first excavation step is performed, this is done using the ramp, load function, presented in Table 7.5.

## 3. Time Dependent

The calculations in time steps 4 to 6 are performed in the same manner as the calculations in step 2 using a time dependent solver. The reason to have two different time dependent solvers is that during time steps 4 to 6 when the pre stressing of the anchor is done as well as the last excavation the time increment needs to be smaller for the calculation to converge.

## 4. Stability Analysis

The last calculation step is a stability analysis, there exists three different types of stability analysis in Z-soil. The stability analysis is optional and is used to create reliable assessments of safety factors and failure surfaces. The stability analysis used for this calculation reduces both the cohesion and the internal friction angle.

## 7.5 Comsol Multiphysics

As Comsol Multiphysics is a general finite element program, there exists none, or at least no generalized method has been found, to simulate the excavation. Therefore it has to be stressed that the methods used may not be the only or most effective manner in which to solve the simulation of this excavation problem.

In Comsol multiphysics the calculations have been performed using the Geomechanics Module, which is an optional package to the Structural Mechanics Module, together with the Subsurface Flow Module. The calculations have been performed in 5 calculation steps according to Figures 7.2-7.6, in a similar procedure to the ones in both Plaxis 2D and Z-soil.

In Comsol Multiphysics the boundary conditions and material properties are established under so called physics, one thing that has made the simulation in Comsol more time consuming than in Plaxis and Z-soil is that no way of turning parts of the geometry on and off during calculations has been found. Instead one of these physics has been established for each of the calculation steps presented in Figure 7.2-7.6. The physic used to control the boundary conditions and material properties for the soil and retaining wall is called *Solid Mechanics*. In addition to establishing these five physics two physics need to be established to calculate the pore water pressure distribution and two physics to simulate the anchoring. The physic used to calculate the pore water pressure is called *Darcy's law* and the physic used to simulate the anchor is called *Truss*.

### 7.5.1 Geometry model

The geometry model used in the calculations is similar to the ones used in Z-soil and Plaxis 2D with one difference, the retaining wall is simulated as a surface and not with beam elements. The geometry model used is displayed in Figure 7.12.



Figure 7.12: *The geometry model used in Comsol Multiphysics.*

In Comsol Multiphysics triangular elements have been used to simulate the soil, whereas structured mesh elements are used for the concrete in the retaining wall. The element mesh used in Comsol is presented in Figure 7.13 and Figure 7.14.

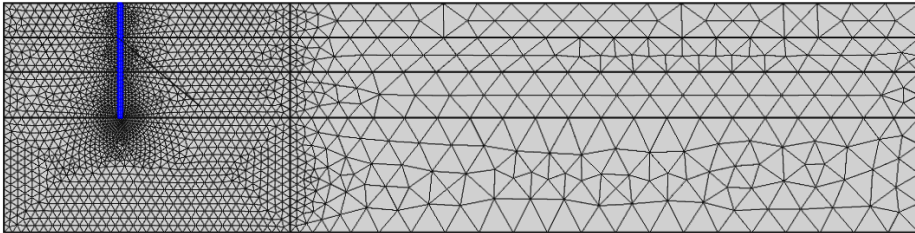


Figure 7.13: *The element mesh used in the Comsol Multiphysics calculations.*

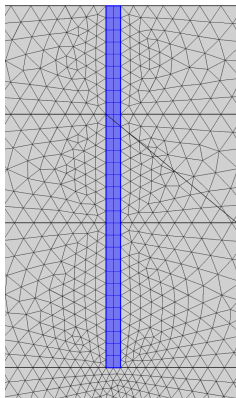


Figure 7.14: *The element mesh distribution around the retaining wall.*

### 7.5.2 Retaining wall

The retaining wall is as mentioned previously simulated as a surface made out of concrete. The boundary between the bottom of the retaining wall and the soil is modeled with a general extrusion operator. This forces the vertical displacement to stay in contact with the soil while the horizontal displacement is unconstrained (Comsol; 2011).

The interaction between the soil and the retaining wall is modeled with a thin elastic layer. The Thin Elastic Layer feature has elastic and damping boundary conditions and acts between two parts and decouples the displacements between two sides of a boundary. The two boundaries are then connected by elastic and viscous forces with equal size but opposite directions, proportional to the relative displacements and velocities (Comsol; 2011). The force between the two parts are governed by a spring force, which can be written as

$$f_{sd} = -f_{su} = -K(u_d - u_u - u_0) \quad (7.2)$$

The spring force has been set to  $K_x = 1 \cdot 10^9$  and  $K_y = 4 \cdot 10^5$ . For more information on the Thin Elastic Layer the reader is referred to Comsol (2011).

### 7.5.3 Pre-stressed ground anchor

The anchor has been modeled using two five meters long truss elements. The truss element representing the concrete injection has been coupled along its full length to the soil using a general extrusion which forces the displacements to stay in contact in with the soil in both directions. The same method is used to connect the end node of the other truss element to the retaining wall.

The prestressing of the truss element is done by assigning an initial stress according to Table 7.3. For the model to converge a ramp function has been used to increase the pre-stressing force linearly during ten incremental steps.

### 7.5.4 Calculations

For each calculation step presented in Figures 7.2-7.6 one solver, or study as they are called in Comsol, has been established, the resulting stresses and strains have then been used as initial values in the following solver. To get the results to only display the deformations that occur after the equilibrium position, the dependent values function has been activated in the solvers.

One important aspect to get convergence in the calculations is to set the relative tolerance in the stationary nonlinear solvers to a sufficiently small value. In these calculations the value for the relative tolerance has been set to  $1 \cdot 10^{-7}$ .

### **Study 1**

In the first study the in-situ stresses and strains are calculated with the pore pressure distribution calculated using the Darcy's law physic as initial stresses.

### **Study 2**

In the second study the surface representing the retaining wall is given the material properties from Table 7.2.

### **Study 3**

In the third study the first excavation step is performed by deactivating the surface representing the first 3 meters of soil. To get the solver to converge, this can, however not be done in one step. Therefore two boundary forces have been created, one representing the vertical stress levels along the bottom line of the deactivated area and one boundary force representing the horizontal stresses along the retaining wall. These boundary forces are then ramped towards zero using the continuation function in the stationary solver.

### **Study 4**

In the fourth calculation step the truss elements are activated. The prestressing of the truss element is done by assigning an initial stress according to Table 7.3. For the model to converge a ramp function has been used to increase the pre-stressing force linearly during ten incremental steps using the continuation function in the stationary solver.

### **Study 5**

The calculations in the last study are performed in the same manner as the calculations in study 3, but with the surface representing the second excavation step deactivated as well. Also in this step a second pore water pressure distribution

has been calculated, where the ground water level has been lowered inside the excavation pit.

## 7.6 Results

When a finite element calculation like this excavation model is performed a series of results will be obtained, ranging from the stress distribution to groundwater flow. This is one of many advantages using finite element calculations, but it is important to know what results that are important for the current case. For geotechnical calculations it is often the displacements that are of primary interest as finite element models commonly are used for calculations in the serviceability limit state. Another advantage using finite element simulations is that results can be obtained after each calculation step, giving the deformations and stress distributions over time.

For simulations of an excavation like the one modeled in this report the most important results are the displacement of the retaining wall and the force in the pre-stressed anchor truss over time. It is also important to get results concerning the water flow into the excavation pit.

### 7.6.1 Deformation field in the soil

All three softwares have a number of ways to display the deformations in the soil, there are options to show the total displacements, the displacement in only one direction or the deformed geometry, to mention a few of the alternatives presented in the three softwares. Figures 7.15-7.17 display the total displacement distribution in all three softwares after the final calculation is completed.

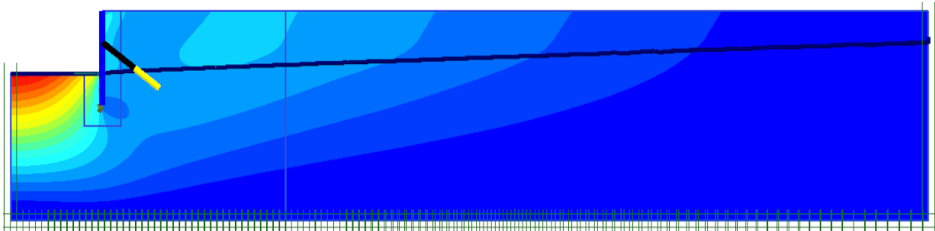


Figure 7.15: *The total displacements after the finished excavation from the calculations done in Plaxis 2D. The largest displacement is 48 mm inside the excavation.*

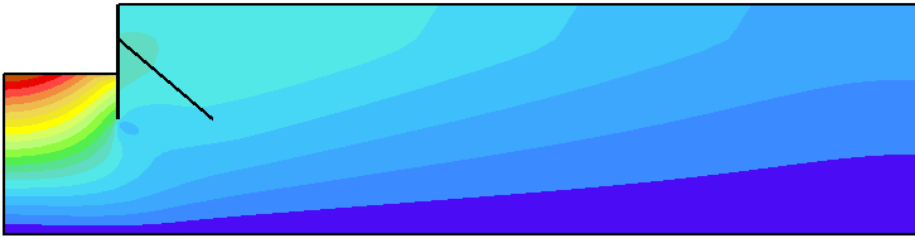


Figure 7.16: *The total displacements after the finished excavation from the calculations done in Z-soil. The largest displacement is 50 mm inside the excavation.*

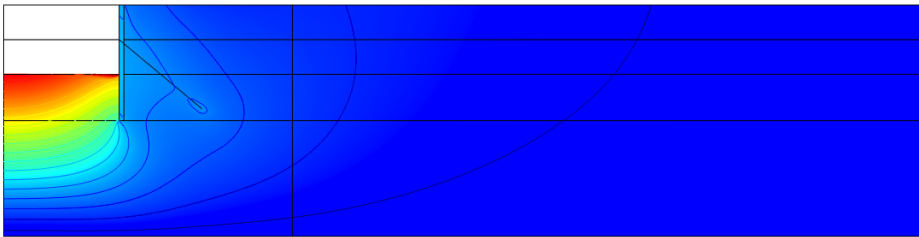


Figure 7.17: *The total displacements after the finished excavation from the calculations done in Comsol Multiphysics. The largest displacement is 59 mm inside the excavation.*

It can be seen in the figures above that the resulting displacements are similar in all three softwares, even though they differ in some ways. One apparent difference obtained from the calculations is that the largest displacement from the Comsol calculations is larger and appears next to the retaining wall and not along the symmetry line as in Plaxis 2D and Z-soil. The displacements along the symmetry line in Comsol does however match the displacements along the symmetry line in Plaxis and Z-soil. The deformations along the retaining wall in Comsol appears to be non-physical. The deformations are shown in Figure 7.18.

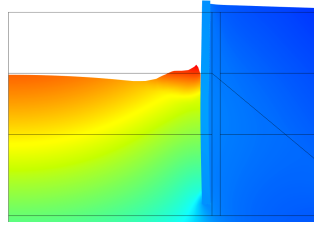


Figure 7.18: *The total displacements from Comsol Multiphysics scaled 50 times the real displacements.*

Why these deformations occur has not been fully concluded. Some possible reasons have been precluded through parameter studies. It has been established that the deformations are not caused by the thin elastic layer, as the contact between the soil and retaining wall has been modeled using other methods as well. Instead a possible reason for the deformation might be that the Mohr-Coulomb criterion in Comsol Multiphysics allows for tensile forces in the soil, which does not appear in most soils. The method used to simulate the excavation by letting a boundary force be ramped towards zero might also be a reason for the deformations displayed in Figure 7.18.

### 7.6.2 Stress distribution

As the strength of a soil depends on the load history it is of importance that the initial effective stress rates are calculated correctly. The horizontal stresses depend on the vertical stresses in both Plaxis 2D and Z-soil, using the  $K_0$  method, see (7.3).

$$\sigma'_{xx} = K_0 \sigma'_{yy} \quad (7.3)$$

In Comsol Multiphysics, on the other hand, the horizontal stresses are calculated using Poisson's ratio. With the values of  $K_0$  and Poisson's ratio according to Table 7.1 the initial horizontal effective stresses are as good as equal in all three softwares. The total vertical stress distribution from Plaxis 2D and the horizontal effective stresses from Comsol Multiphysics are displayed in Figure 7.19 and 7.20.

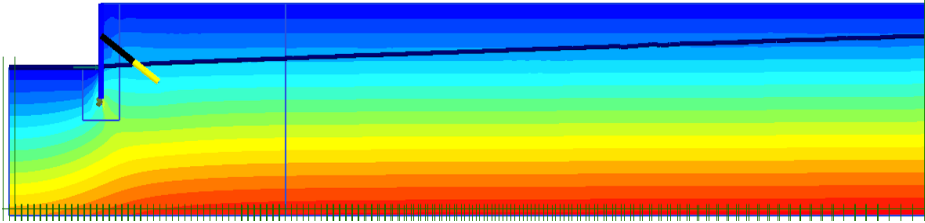


Figure 7.19: *The vertical total stress distribution after the finished excavation from the calculations done in Plaxis 2D.*

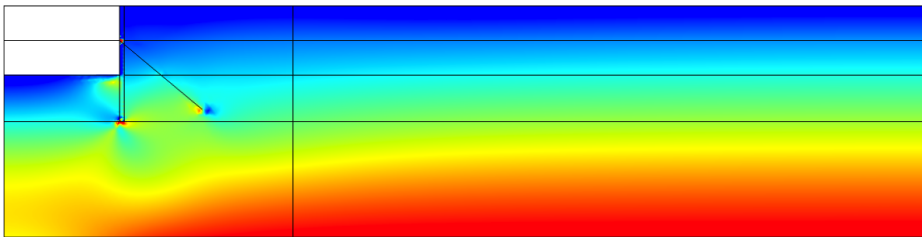


Figure 7.20: *The horizontal effective stress distribution after the finished excavation from the calculations done in Comsol Multiphysics.*

In all three softwares the total vertical stress distribution ranged from 0 kPa at the ground level, to about -425 kPa at the bottom of the model. The corresponding effective stresses ranged from 0 kPa at the ground level, to -240 kPa at the bottom of the model.

The corresponding horizontal total stresses ranged from 0 kPa at the ground level, to -270 kPa at the bottom of the model. The effective horizontal stresses ranged from 0 kPa at the ground level, to -100 kPa at the bottom of the model.

### Plastic zones

One more feature that might be interesting to observe is where the soil have reached failure for the Mohr-Coulomb criterion. The developed plastic zones from the three softwares after the last calculation step can be observed in Figures 7.21-7.23.

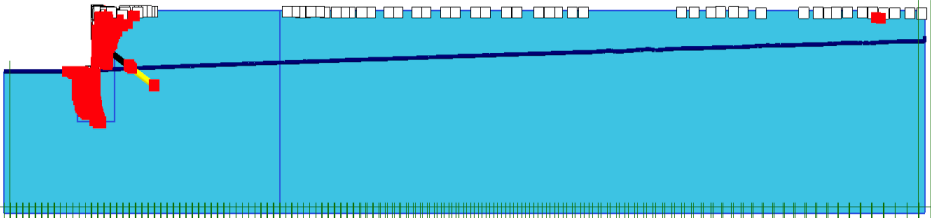


Figure 7.21: *The plastic zones from the calculations done in Plaxis 2D.*

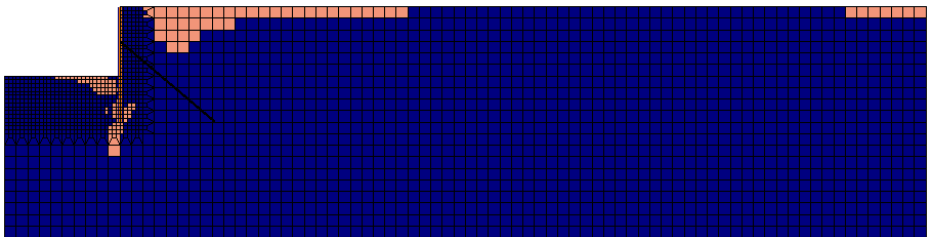


Figure 7.22: *The plastic zones from the calculations done in Z-soil.*

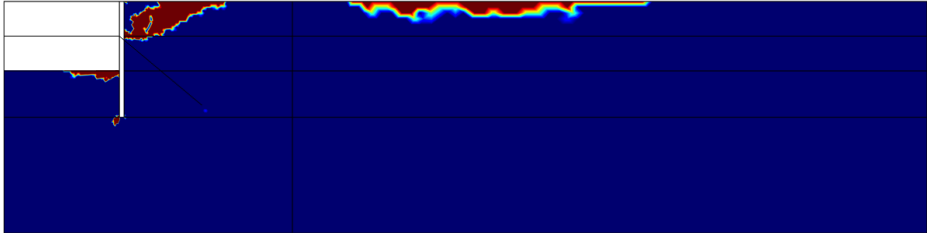


Figure 7.23: *The plastic zones from the calculations done in Comsol Multiphysics.*

It can be seen that some differences exist in where the three softwares have reached the yielding stress. Also all three softwares have generated plastic deformations on the soil surface some way from the retaining wall. These plastic strains are likely to be a result from the fact that the Mohr-Coulomb criterion allows for tensile stresses in the soil that has propagated along the surface in the model.

### 7.6.3 Retaining wall

The displacement of the retaining wall during the excavation process might be the result that is of greatest interest as it is possible to measure during the work at a construction site. In Figure 7.24, the total displacement at the top of the retaining wall is displayed. The fictitious time in the figures can be seen as the calculation steps illustrated in Figures 7.2- 7.6. For example after the time 3 the first excavation step has been completed.

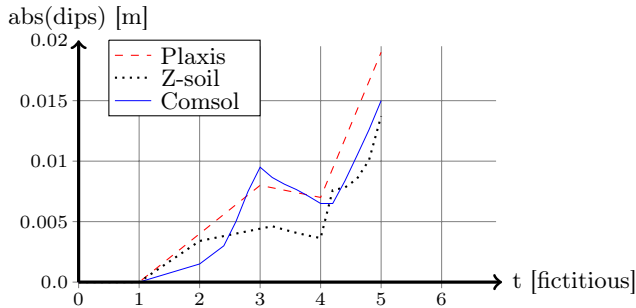


Figure 7.24: *Total displacement at the top of the retaining wall.*

In Figure 7.25 the horizontal displacements at the top of the retaining wall during all the calculation steps are displayed.

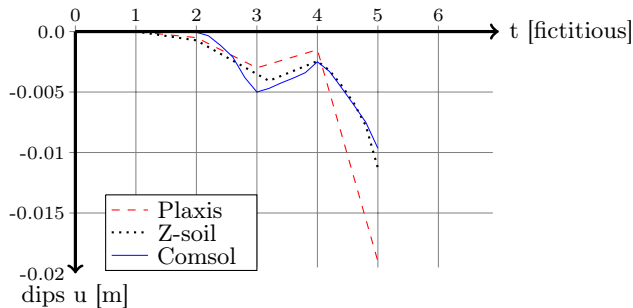


Figure 7.25: *Displacements in x-direction at the top of the retaining wall.*

From the results it can be seen that the retaining wall shows smaller vertical displacements in Z-soil than in Plaxis and Comsol. There are a few possible reasons

for this, even though the retaining wall has been modeled in a similar manner in Plaxis and Z-soil the contact at the bottom has been modeled differently. Secondly, in Z-soil the effects of friction between the retaining wall and the soil is modeled in a more complex way than in Plaxis.

### Forces in the retaining wall

As a beam element has been used to model the retaining wall in Plaxis 2D and Z-soil it is possible to obtain the bending moment and shear force distribution along the retaining wall. The resulting bending moments calculated in Plaxis and Z-soil are almost identical, therefore the bending moment from Z-soil is the only one presented.

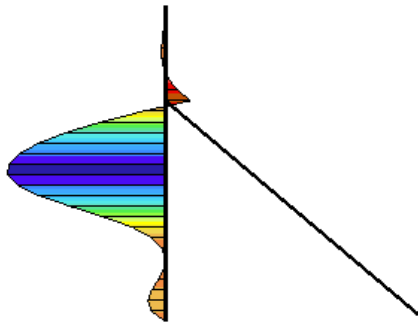


Figure 7.26: *The bending moment for the retaining wall in Z-soil after the completed excavation. The values range from 8.5 kNm to -53 kNm.*

As the retaining wall have been modeled as a surface in Comsol no feature to display the bending moment has been found. However, it is possible to view the stress distribution in the retaining wall, as an example the von Mises stress distribution is displayed in Figure 7.27.



Figure 7.27: *The von Mises stress distribution in the retaining wall, ranging from 8 kPa to 2.3 MPa.*

It should be mentioned that even though the retaining wall has been modeled in a different manner in Comsol than in Plaxis and Z-soil the displacements at the top of the wall are quite similar in all three softwares. It also needs to be said that the retaining wall could have been modeled using a beam element in Comsol as well. Due to time and convergence problems that method has not been explored during the work with this report.

#### 7.6.4 Anchor force

Another important result from the calculations is the force in the pre-stressed anchors during the excavation steps as this is one parameter that is relatively easy to evaluate while the excavation is taking place. In Table 7.7 the force in the anchoring bar from each software is displayed.

Table 7.7: Force level in the anchoring brace at installation and at end of excavation.

Calculation step	Plaxis	Z-soil	Comsol
Force level at step 4 [kN]	75	75	78
Force level at step 5 [kN]	91	93	100

In Figure 7.28 the displacements in the node where the anchor is attached to the retaining wall is presented.

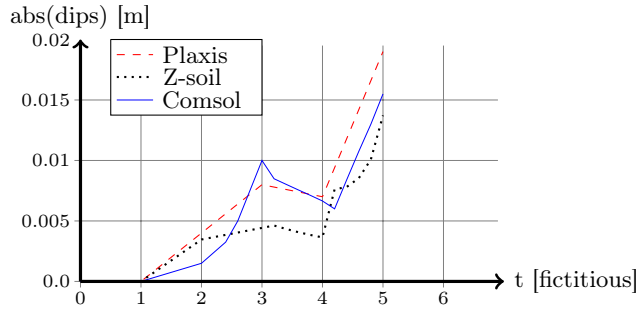


Figure 7.28: *Total displacement at the node where the anchoring brace is attached to the retaining wall.*

From the results it can be seen that the force levels in the anchor elements are quite similar, even though the anchors have been modeled in different ways in the softwares. That Z-soil again displayed smaller displacements than the other softwares is believed to be due to the reasons discussed regarding the retaining wall earlier.

## 7.7 Discussion

From the calculations of the idealized excavation problem presented in this chapter it can be concluded that all three softwares can be used to perform this type of geotechnical calculations. But at the same time that even though the models have been made as similar as possible in all three softwares some differences will exist and influence the results.

A few of these differences are due to how certain aspects of the excavation problem have been modeled, i.e. the retaining wall, the pre-stressed anchor or the ground water. Other differences are more due to the softwares themselves, such as the element types and solvers used in the calculations. However, the biggest differences between the three softwares lies in the manner in which elements are activated or deactivated during the calculation procedures.

Another important aspect when performing finite element calculations is the time needed to establish the model. This is naturally an aspect that depends on how well the user handles the software at hand and in somewhat a speculative aspect. However, the differences in time needed to establish a working model for the

excavation problem at hand have been rather large, and therefore needs to be addressed.

That it is fast and easy to establish a model is certainly one of the benefits of using one of the specialized geotechnical finite element softwares, Plaxis 2D or Z-soil. However, it is a bit unfair to judge the time taken to establish this excavation problem as a general evaluation of this aspect. The fact that Plaxis 2D and Z-soil have a set of typical geotechnical problems presented in their tutorials also helps the user when problems arise. That only a few example models regarding geotechnical problems are presented in Comsol Multiphysics leads to that the user needs to have more extensive knowledge of the software and finite element calculations to create a model.



## 8 Conclusions and suggestions for further work

As the goal with this report is to evaluate Plaxis 2D, Z-soil and Comsol Multi-physics this chapter will discuss the experience using the three softwares. Therefore some pros and cons that have been experienced with the three softwares will be pointed out in the following.

### **Plaxis 2D**

The greatest benefits with using Plaxis 2D compared to Z-soil and Comsol Multi-physics is that less time is needed to establish a working finite element model. It also demands considerably less knowledge about finite element calculations from the user than the other softwares do.

The biggest disadvantage when using Plaxis 2D is, that although there exists elements to model beams and trusses, there are limitations to the possibilities for modeling construction-soil interactions.

Thanks to the usability in Plaxis 2D it may be used to perform both smaller problems that usually are performed by hand calculations as well as idealized more conventional two-dimensional plane strain calculations.

It can also be seen as negative that Plaxis is divided into several smaller programs, i.e. Plaxis 2D, Plaxis 3D as well as dynamic and flow versions in both two and three dimensions.

### **Z-soil**

Setting up a model in Z-soil is more complex and time consuming than in Plaxis 2D. In Z-soil however, there exists a better way to get an overlook of the calculations through a method to visualize which elements and surfaces that are active in each calculation step. This makes it possible to step through both geometrical and physical changes over time before initializing the calculations. It is therefore possible to notice if something looks strange in the model before initializing the calculations, and hence save time.

Z-soil also contains more possibilities than Plaxis 2D when it comes to modeling other construction parts interacting with the earth materials. Where the most obvious advantage is that surface elements can be created to model large constructions, such as dams, tunnels or concrete slabs.

The biggest setback experienced with Z-soil is that it is complicated and rather time consuming to make changes in the geometry after that the element mesh has been generated. This has to do with that Z-soil splits all surfaces into elements, making it possible to change features in each element separately making an altering of the geometry complicated.

### **Comsol Multiphysics**

As Comsol Multiphysics is a general finite element software, there are endless possibilities for the user when setting up a model. This diversity however, does not always play in Comsol's favor when establishing a simple idealized model.

There are on the other hand numerous more possibilities with a general finite element software such as Comsol. The fact that Comsol allows the user to add on physical effects gradually also gives the user means to study more complex problems without the need of building a new model in another finite element software. These features do however not come to its right in a small problem as the model used in this report.

That no generalized method on how to solve excavation types of problems, i.e. how parts of the geometry are activated or deactivated during the calculations, is presented in Comsol Multiphysics is perhaps the single disadvantage using the program compared to Z-soil and Plaxis 2D. Many different methods and features in Comsol Multiphysics have been tested to accomplish these geometrical and physical changes during the work with this report, and the method presented in Chapter 7 was the only one of the tested procedures that worked satisfactory.

That been said, there might exist functions in the software to accomplish this in a better way than presented in this report.

Another feature that would have simplified the modeling of groundwater flow in the software would have been to use the Poroelasticity physic together with soil plasticity, something that was not feasible in the version used for this evaluation.

### **Summary and suggestion for further work**

From the work presented in this report it can be summarized that all three softwares can be used for geotechnical calculations, and that for small and rather simple models Plaxis 2D is probably the software to prefer even though Z-soil might work just as well if the user is familiar with the software. If a more complex study is to be performed, where effects of other materials and the interaction between these materials and soils are of importance, then Z-soil or Comsol Multiphysics both would work.

As this evaluation was done as a master's dissertation, time has been a limit on how this evaluation has been performed. It would therefore be interesting to conduct some further work to extensively compare the functionality and possibilities for geotechnical calculations. It would for example be interesting to evaluate how the softwares perform in a larger more complex three-dimensional simulation, where more complex material models could be used, as well as a means of adding on more physical aspects, i.e. thermal and dynamic effects.



# Bibliography

- Brinkgreve, R. (2011). *Plaxis 2D Reference Manual*, Plaxis bv P.O. Box 572, 2600 AN DELFT, Netherlands.
- Comsol (2011). *COMSOL Multiphysics User's Guide*, comsol 4.2a edn, COMSOL AB, COMSOL AB, Tegnérgatan 23, SE-111 40 Stockholm.
- Desai, C. S. and Siriwardane, H. J. (1984). *Constitutive laws for engineering materials, with emphasis on geologic materials*, Prentice-Hall, Englewood Cliffs, N.J.
- Jönsson, D. (2007). *Konstruktion i samverkan - utvärdering av olika fe-program*, Master's thesis, Division of Structural Mechanics, LTH, Lund University, Box 118, SE-221 00 Lund, Sweden.
- Mitchell, J. K. and Soga, K. (2005). *Fundamentals of soil behavior*, 3rd edn, John Wiley and Sons, Hoboken, N.J.  
**URL:** <http://www.loc.gov/catdir/toc/ecip053/2004025690.html>
- Ottosen, N. S. and Ristinmaa, M. (2005). *The mechanics of constitutive modeling*, first edn, Elsevier, The Boulevard, Langford Kidlington, Oxford OX5 1GB UK.  
**URL:** <http://www.loc.gov/catdir/enhancements/fy0632/2006273557-d.html>
- Zace Services Ltd, S. e. (2003). *Z SOIL.PC User Manual Theory*, P.O.Box 2, 1015 Lausanne, Switzerland.